

RESEARCH

Open Access



Fibroblast IRF7-mediated chondrocyte apoptosis affects the progression of collapse in steroid-induced osteonecrosis of the femoral head

Han Longfei^{1†}, Fang Weihua^{1†}, Han Mingli¹, Zhuang Zhikun^{4*}, He Mincong^{2,3*} and Wei Qiushi^{2,3*}

Abstract

Purpose The objective of this study was to identify potential genes implicated in the “peri-collapse” synovium of osteonecrosis of the femoral head through coding gene sequencing and to further clarify their specific mechanisms via in vitro experiments.

Methods Steroid-induced osteonecrosis of the femoral head (SIONFH) ($n=3$), femoral neck fracture (FNF) ($n=3$), and hip osteoarthritis (HOA) ($n=3$) Synovial tissue of the hip joint was collected in total hip arthroplasty. A cellular model of SIONFH constructed from rat synovial fibroblasts by lipopolysaccharide intervention. Lentiviral technology was used to construct a model for fibroblast knockout of the *Irf7* gene. HE was used to compare the characteristics of synovial tissue damage, and immunofluorescence and immunohistochemistry were used to compare the expression levels of VIM, IRF7, and IFN α . PCR, WB, and IF were used to examine *Irf7* knockdown efficiency, chondrocyte proliferation (Col2a1, Aggrecan, Sox9), cartilage matrix degradation (Mmp13), and apoptosis (Bcl2, Bax, and Caspase3) expression under co-culture conditions. Crystalline violet staining was used to observe the migration rate of fibroblasts, and flow cytometry was used to detect the apoptosis level of chondrocytes under co-culture conditions.

Results Transcriptome sequencing of synovial tissue and fibroblasts ultimately screened for six differential genes, HOOK1, RNPC3, KCNA3, CD48, IRF7, SAMD9. Compared to FNF and HOA, synovial inflammatory cell recruitment and synovial hyperplasia were more pronounced in SIONFH. IF and IHC confirmed high expression of IRF7 and IFN α in the synovium of SIONFH. PCR and WB results suggested that fibroblasts highly expressed *Irf7*, *Hook1*, *Rnpc3*, *Kcna3*, *Cd48*, *Samd9*, *Il-6*, and *Tnfa* after lipopolysaccharide intervention, and the expression levels of *Il-6* and *Tnfa* were significantly reduced after knockdown of *Irf7* ($P < 0.001$). In the co-culture system, fibroblasts intervened with lipopolysaccharide

[†]Han Longfei Fang Weihua and contributed equally to this work.

*Correspondence:

Zhuang Zhikun

qiflynn@163.com

He Mincong

mincong.he@hotmail.com

Wei Qiushi

weiqushi@126.com

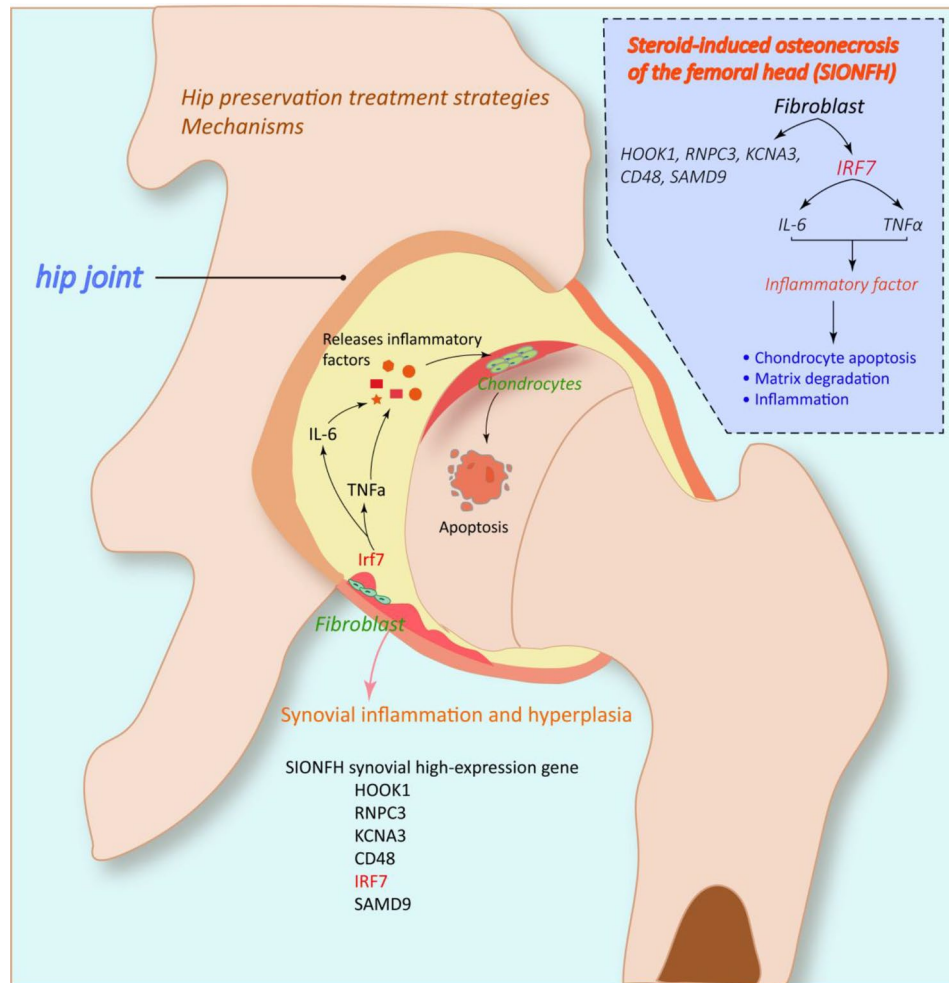
Full list of author information is available at the end of the article



significantly promoted chondrocyte apoptosis, the rate of cartilage matrix degradation, while inhibiting the level of chondrocyte proliferation, and this result was significantly reversed in *Irf7* knockout fibroblasts. This was supported by flow cytometry results.

Conclusions IRF7, HOOK1, RNPC3, KCNA3, CD48, and SAMD9 as potential genes affecting the progression of SIONFH collapse. *Irf7* mediates the fibroblast inflammatory response and affects the collapse process of SIONFH by influencing chondrocyte apoptosis. Thus, intervention in IRF7 holds promise as one of the key targets for reversing the collapse process of SIONFH.

Graphical Abstract



Keywords Gene expression profiles, Steroid-induced osteonecrosis of the femoral head, Apoptosis, Synovial fibroblasts, Collapse

Introduction

Osteonecrosis of the femoral head is a severely debilitating condition that can be classified as either traumatic or nontraumatic. Steroid-induced osteonecrosis of the femoral head (SIONFH) occurs due to excessive glucocorticoids use and is associated with a high disability rate, primarily affecting young and middle-aged individuals. Once this condition manifests, it significantly impairs

the patient's daily activities, leading not only to substantial social burdens but also to devastating consequences for the patient's family [1]. Regarding pathogenesis, it is widely accepted that hemodynamic changes constitute the primary causative factor, resulting in the temporary or permanent loss of blood supply to the femoral head [2, 3]. Osteocellular necrosis leads to a reduction in mechanical strength of the femoral head, subsequently resulting

in collapse and ultimately secondary hip osteoarthritis [4, 5]. Multiple treatment options exist for ONFH [6–10]; however, each has its limitations. Commonly employed treatments for ONFH include free fibula graft (FFG), free vascularized fibula graft (FVFG), extracorporeal shock wave therapy (ESWT), autogenous iliac bone graft (ABG), core decompression (CD), multiple drilling decompression (MDD), and intraosseous drug injection therapy (IDIT) [1]. However, the long-term benefits of these treatments are limited, and eventual hip replacement may be unavoidable [11]. A bioinformatics approach aimed at identifying key genes associated with SIONFH and intervening in its progression represents a promising novel therapeutic modality for reversing osteonecrosis. RNA sequencing is a powerful tool for quantifying RNA expression with high sensitivity across the genome [12, 13]. In recent years, this technology has been utilized in the study of femoral head necrosis. The sequencing samples include Latrunculin A-treated adipocytes [14], subchondral bone from human femoral heads [15, 16], exosomes secreted by human umbilical cord mesenchymal stem cells [17], glucocorticoid-treated human umbilical vein endothelial cells [18], and patient blood serum [19]. This research incorporates both coding and noncoding genes to screen for key targets.

The synovium of the hip constitutes a neglected yet critically important aspect of osteonecrosis of the femoral head (ONFH). Research indicates that ONFH is frequently associated with chronic synovial inflammation, predominantly observed during the middle to late stages of the condition [20, 21]. Hip synovitis primarily occurs during the “peri-collapse” phase of ONFH [22, 23], when microfractures within the femoral head generate intracapsular inflammatory factors that irritate the synovium, thereby exacerbating the progression of the collapse. Consequently, in patients with early-stage ONFH collapse, intervention on the synovium and hip-preserving surgery are anticipated to become significant strategies for maintaining hip function. Notably, chronic synovitis is more prevalent among children with Legg-Calvé-Perthes disease (LCPD) [24]. Given that the synovium and femoral head are enclosed within the hip joint capsule, synovitis is highly likely to impact the femoral head, resulting in pathological changes primarily reflected in the biochemistry of the femoral head cartilage, mechanical properties, joint biomechanics, and overall prognosis [25]. Untreated synovitis may result in pathological processes including cartilage edema, reduced mechanical properties of the cartilage, excessive cartilage metabolism, and chondrocyte hypertrophy and apoptosis, potentially leading to severe clinical symptoms such as femoral head deformation, collapse, and lateral subluxation. Although synovial inflammation is not a primary pathological change in SIONFH, its control is crucial for ensuring the efficacy of

hip preservation therapies. Nonetheless, the role of synovitis in the progression of ONFH remains unclear. Thus, this study focuses on the SIONFH synovium to elucidate synovial differential gene expression in SIONFH patients through RNA sequencing and to further investigate the downstream mechanisms experimentally.

Interferon regulatory factors (IRFs) play a crucial role in innate receptor signaling and are responsible for inducing type I interferon (IFN) responses downstream of pattern recognition receptors. IRF3 and IRF7 are key regulators of type I interferons [26, 27]. The IRF and IFN families are critical in regulating the viral response, whereby the nuclear translocation of IRF7 induces the expression of the IFN β gene and several isoforms of the IFN α gene, thereby modulating the viral response. Lansoprazole has been reported to inhibit IRF7 activity, potentially preventing corticosteroid-induced ONFH in rat models, and has been shown to significantly reduce the incidence of ONFH in patients with autoimmune diseases following corticosteroid therapy in clinical trials [28]. Additionally, IRF7 promotes the progression of ONFH by mediating TLR7 or TLR9 and MyD88, which in turn affects the expression of pro-inflammatory signaling transcription factors [29]. This suggests that IRF7 is closely related to the development of ONFH; however, the role of the IRF7 gene in hip synovial fibroblasts has not been investigated. In this study, we focused on the downstream mechanisms of IRF7 based on the sequencing results to elucidate its critical role in influencing the progression of SIONFH. Maintaining homeostasis in cell proliferation and apoptosis is essential for growth, development, and overall physiological equilibrium [30, 31]. Typical manifestations of apoptosis, which help maintain homeostasis within the organism, include rounding and crumpling of cells, fragmentation of DNA, and the formation of apoptotic vesicles that are subsequently cleared by macrophages. An imbalance in the homeostasis of cell proliferation and apoptosis can lead to various human diseases [32] (Table 1).

This study aimed to investigate synovial differential gene expression in the hip joints of patients with SIONFH and to explore potential therapeutic targets. We conducted a combined analysis of RNA sequencing results from human synovial tissue and *in vitro* cultured fibroblasts to elucidate the differential expression of genes associated with SIONFH in the hip synovium. Subsequently, we screened six differential genes, including HOOK1, RNPC3, KCNA3, CD48, IRF7, and SAMD9. We established a co-culture system to facilitate direct contact between synovial fibroblasts and chondrocytes while silencing *Irf7* gene expression using gene silencing technology. The apoptotic indexes of chondrocytes were subsequently examined, revealing that *Irf7* in fibroblasts mediates chondrocyte apoptosis, thereby promoting the

Table 1 Information on patients

Serial number	Group	Genders	Age	diagnosis
1	FNF1	male	45	Left femoral neck fracture
2	FNF2	female	50	Left femoral neck fracture
3	FNF3	female	55	Right femoral neck fracture
4	HOA1	male	59	Left hip osteoarthritis
5	HOA2	male	60	Right hip osteoarthritis
6	HOA3	female	62	Left hip osteoarthritis
7	SIONFH1	female	36	Bilateral steroid-induced osteonecrosis of the femoral head
8	SIONFH2	male	30	Bilateral steroid-induced osteonecrosis of the femoral head
9	SIONFH3	female	34	Bilateral steroid-induced osteonecrosis of the femoral head

progression of SIONFH collapse. Thus, the results of this study suggest that anti-inflammatory therapy targeting IRF7 may represent a beneficial therapeutic strategy for the treatment of SIONFH.

Methods

Patients and sample collection

The study received approval from the Ethics Committee of the Third Affiliated Hospital of Guangzhou University of Chinese Medicine (Approval No. PJ-XS-20230523-002). Three patients with SIONFH, three with hip osteoarthritis (HOA), and three with femoral neck fracture (FNF) were recruited for this study between December 13, 2021, and April 10, 2022. Previous studies indicate that ONFH can result in osteonecrosis around the hip joint and cartilage degeneration of the femoral head, potentially leading to femoral head collapse and degenerative arthritis [33–35]. To mitigate the influence of HOA on the results, we included HOA samples in the study. Patients with femoral neck fractures (FNF) who did not exhibit a concurrent inflammatory response served as the control group. Synovial tissue from all groups was obtained from patients undergoing total hip arthroplasty. All patients provided informed consent for the use of their clinical information in scientific research.

1) Human Synovium Acquisition: Removal of synovium from the hip joint capsule was performed using standardized surgical techniques. Fresh synovial tissue, approximately 2 cm² in size, was excised from each patient, immediately placed on dry ice, and total RNA was extracted from the tissue using TRIzol reagent.

2) Intervention and Collection of Cell Samples: To screen for key genes associated with osteonecrosis of the femoral head at the cellular level, a cellular model of steroid-induced osteonecrosis was developed by treating

rat synovial fibroblasts with 5 µg/ml lipopolysaccharide (LPS) for 48 h. Rat synovial fibroblasts were cultured in a medium containing 10% fetal bovine serum, 1% penicillin/streptomycin, and 1% fibroblast growth factor in an incubator maintained at 37 °C with 5% CO₂. Cells were collected after 48 h of intervention, during which lipopolysaccharide was added at a final concentration of 5 µg/ml. Control cells, which did not receive lipopolysaccharide intervention, were collected simultaneously, with three biological replicates obtained from each sample group.

Analysis of sequencing data

RNA quantification and qualification

RNA integrity was assessed using the RNA Nano 6000 Assay Kit with the Bioanalyzer 2100 System (Agilent Technologies, CA, USA).

Differential expression analysis

Differential expression analysis across three conditions (three biological replicates per condition) was conducted using the DESeq2 R package (version 1.20.0). The DESeq2 package provides statistical routines for determining differential expression in digital gene expression data using a model based on the negative binomial distribution. The resulting p-values were adjusted using the Benjamini and Hochberg approach to control the false discovery rate. Genes identified by DESeq2 with an adjusted p-value < 0.05 were classified as differentially expressed.

GO and KEGG enrichment analysis of differentially expressed genes

Gene Ontology (GO) enrichment analysis of differentially expressed genes was conducted using the clusterProfiler R package, in which gene length bias was corrected. GO terms with a corrected p-value of less than 0.05 were considered significantly enriched by differentially expressed genes. The Kyoto Encyclopedia of Genes and Genomes (KEGG) is a database resource designed to facilitate the understanding of high-level functions and utilities of biological systems, including cells, organisms, and ecosystems, from molecular-level information, particularly large-scale molecular datasets generated by genome sequencing and other high-throughput experimental technologies (<http://www.genome.jp/kegg/>). We utilized the clusterProfiler R package to test the statistical enrichment of differentially expressed genes in KEGG pathways.

Reagents and instruments

Healthy rat synovial fibroblasts (iCell Bioscience); Rat Synovial Fibroblast Medium (iCell Bioscience); DMEM/F12 complete medium (GIBCO); Lipopolysaccharides

from *Escherichia coli* O111:B4 (Sigma-Aldrich); TRIzol (Beyotime); Evo M-MLV RT Premix for qPCR and SYBR Green Premix Pro Taq HS qPCR Kit (Rox Plus) (Accurate Biology); Trypsin(Biosharp); PBS(Procell); Puromycin(Ligatrap); ANNEXIN V- FITC/PI Apoptosis Detection Kit(Solarbio); Goat Anti-Rabbit Antibody, Gapdh, Il-6, Tnf α , Aggrecan, Sox9, Mmp13, Bcl2, Bax, Caspase3, Col2a1, Goat Anti-Rabbit IgG (H+L) CY3(All are Affinity); Irf7 Antibody(ProMab); Enzyme Labeler Model 550 (BioRad USA); RTG50005-9-VBC Carbon dioxide incubator (ThermElectron, USA); IX-71 Inverted Microscope (Olympus, Japan); Western Blot Instruments (Bio-Rad PowerPac); Micropipettes (Eppendorf, Germany); Benchtop High-Speed Freezing Centrifuge(Ther&Fisher Scientific USA); Leica inverted fluorescence microscope (Caikgn, China); Full-wavelength enzyme labeller (Ther& Fisher Scientific, Bio-rad, USA); Fluorescence quantitative PCR instrument (ABI, USA); ChemiDoc XRS System (Bio-Rad); Analytical Flow Cytometer(Becton, Dickinson and Company).

Experimental technique

Extraction of rat chondrocytes

We euthanized two 4-week-old SD rats using an overdose of anesthesia, and the cartilage from the rat's knee was removed in a sterile environment. The tissue was rinsed in PBS containing penicillin/streptomycin, cut into 2–5 cm² sections, treated with trypsin, and incubated for 30 min. The digestion was terminated by adding twice the volume of culture medium, followed by centrifugation at 1000 rpm for 5 min, and the precipitate was washed twice with PBS. Type II collagenase was added and incubated for 10 h, followed by filtration through a sieve with a pore size of 70 μ m. The filtrate was collected into a centrifuge tube, centrifuged at 1000 rpm for 5 min, and the precipitate was resuspended in culture medium to obtain the extracted chondrocytes.

Establishment of the transwell co-culture system

A total of 1×10^4 fibroblasts and chondrocytes were uniformly inoculated in Transwell chambers, with fibroblasts seeded in the upper chamber and chondrocytes in the lower chamber, separated by a 0.4 μ m PET membrane that permitted liquid passage while preventing cell movement. The upper and lower chambers were assembled, and cell cultures were maintained under aseptic conditions throughout the experiment. Fibroblasts were pretreated with lipopolysaccharide (LPS) for 48 h before being seeded into Transwell chambers. Fibroblast medium was added to the upper chamber, and DMEM/F12 medium was added to the lower chamber. After a total incubation period of 48 h, chondrocytes were collected from the lower chamber for subsequent analysis.

Irf7 knockout

Lentiviral vectors were developed in collaboration with Shanghai Gikai Genetics. Fibroblasts were inoculated into 24-well plates at a concentration of 5×10^4 cells/mL. Lentivirus at a titer of 1×10^8 TU/mL was added after 1 day, the medium was changed after 16 h, and the culture continued for 72 h. The fluorescence expression of the cells was then observed using inverted fluorescence microscopy. Cells were collected, and puromycin was added at a concentration of 2.5 μ g/mL. Following 48 h of incubation, cells were collected for verification of knock-down efficiency and subsequent experiments.

Crystalline violet staining of fibroblasts

Crystal violet staining was employed to facilitate cell counting and assess the migratory capacity of fibroblasts. An equivalent number of fibroblasts from the control group, LPS intervention group, knockout group, and knockout-control group were collected and seeded into the upper chamber of the Transwell, which had a membrane pore size of 8 μ m to allow cell passage. Serum-free medium was added to the upper chamber, while serum-containing medium was added to the lower chamber, and the chambers were incubated for 48 h at 37 C° in a 5% CO₂ atmosphere. The medium was discarded, and the lower layer of cells was washed three times with cold PBS before being fixed immediately with 4% paraformaldehyde for 15 min. The paraformaldehyde was discarded, and the cells were washed three times with PBS before being stained with crystal violet solution for 15 min. Subsequently, the cells were washed once with PBS, observed, and recorded using an inverted fluorescence microscope (Table 2).

Western blot

The cells in each group were washed three times with pre-cooled PBS, and the protein was extracted with RIPA and protease inhibitor (PMSF), and the protein concentration was determined using a Microplate reader. An aliquot of protein sample was taken for electrophoresis (120 V for 45 min), and the bands were transferred to the membrane at 100 V for 100 min and immersed for 30 min in a rapid Blocking solution. Irf7, Il-6, Tnf α , Col2a1, Aggrecan, Mmp13, Bcl2, Bax, Caspase3 antibodies were added and incubated overnight at 4 °C in the refrigerator. After 8 h, the antibody was recovered and washed with TBST for 3 times, then the secondary antibody was added and incubated at room temperature for 1 h, then washed with TBST again, and finally the protein expression was observed.

RNA extraction and RT-qPCR

The RNA of the cells was extracted using the Animal Tissue RNA Extraction Kit (Biyun Tian), reverse transcribed

Table 2 Primer sequence list

Gene	Primer sequence (5'→3')
Gapdh	F: GGGTCCCAGCTTAGGTTTCAT R: TACGGCCAAATCCGTTTCACA
Irf7	F: CAGCCGTAGGGATCTGGATG R: CAAGATAAAGCGCCCTGTGC
Il-6	F: CCAGTTGCCTTCTTGGGACT R: CTGGTCTGTTGTGGGTGGTA
Tnfa	F: GGAGGGAGAACAGCAACTCC R: GCCAGTGATGAGAGGGACG
Col2a1	F: CACCGCTAACGTCCAGATGA R: GTTTCGTGCAGCCATCCTTC
Aggrecan	F: GCCTCCCTGATCCACTGTCC R: ATGTCAGAGGGCGATGTGGG
Sox9	F: TGAAGTGACCGACGAGCAG R: GTCCAGTCGTAGCCCTTCAG
Mmp13	F: TTCTGGTCTTCTGGCACACG R: TGGCTTTTGCCAGTGTAGGT
Bcl2	F: TGACTTCTCTCGTCCGCTACCGT R: CCTGAAGAGTTCTCCACCACC
Bax	F: GCAGGCATGTGGAGAGTGAAC R: CTGGCGAAGAGAGACTTTGTGTG
Caspase3	F: AGCCACGGTGATGAAGGAGTC R: GCCTCGGCAAGCCTGAATAATG
Rnpc3	F: ACACCGTTTGGACCGATTAC R: GTTGAGGTGATGATAGGTGGAAG
Hook1	F: GGAGTACAGAGAGGTGTTTCATT R: CGTTCATCTTGGCGTGTTC
Kcna3	F: TGCTGCGATTCTTCTTCCTTGC R: GCGGAAGACCCTTACTAGGC
Cd48	F: CACTCCACACAACAAGTCTACA R: CCAGCGTACAAGGTGGAATAA
Samd9	F: CCGATTGCTTACAGCTTGATG R: CATCTTGTAGTGACGGTGGTGAG

to cDNA, and stored at -20°C . Irf7 was used to validate the knockdown efficiency, Il-6, Tnfa was used to detect the inflammation level of fibroblasts, Col2a1, Aggrecan, Sox9 was used to detect the proliferation level of chondrocytes, Mmp13 was used to detect the matrix degradation level of chondrocytes, Ccl2 was used to detect the inflammation level of chondrocytes, and Bcl2, Bax, Caspase3 was used to detect the apoptosis level of chondrocytes. Real-time quantitative assays were performed for each gene, and reactions were performed in a fluorescence quantitative PCR instrument. Primer sequences are shown in Table.

Flow cytometry to detect apoptosis levels

Flow cytometry was used to detect the apoptosis rate of chondrocytes in the co-culture system. Cells were digested by trypsin (without EDTA) and collected in centrifuge tubes, Binding Buffer was added to adjust the cell concentration to $5 \times 10^6/\text{ml}$. Take 100ul cell suspension and add 5ul Annexin V/FITC to incubate at room

temperature and avoid light for 5 min, add 5ul propidium iodide solution (PI), add 400ul PBS, and immediately on the machine for apoptosis rate detection.

HE staining of synovium

The synovial tissue was paraffin-embedded and sectioned, left to stand at 60°C for 30 min, deparaffinised by xylene, and placed in anhydrous ethanol for 3 minx3 times, 90%, 80% and 70% ethanol in that order, each for 3 min. Distilled water washes for 5 min and HE staining was performed. After dehydration with graded concentrations of ethanol and xylene transparency, the slices were sealed with neutral gum and placed under a microscope.

Immunofluorescence & immunohistochemistry

Tissue immunofluorescence: The synovial tissue was paraffin-embedded and sectioned, left to stand at 60°C for 30 min, deparaffinised by xylene, and placed in anhydrous ethanol for 3 minx3 times, 90%, 80% and 70% ethanol in that order, each for 3 min. Sections were repaired by sodium citrate buffer for 10 min, washed in PBS, and immersed in 0.1% Triton X-100 for 10 min to permeabilise the cell membrane. Add goat serum and soak at room temperature for 2 h, add primary antibody and incubate at 4°C overnight, wash with PBS and add fluorescent secondary antibody and incubate at room temperature for 1 h, add DAPI and incubate for 5 min, observe and record under fluorescence microscope.

Cell immunofluorescence: When the cell density reached 80%, the cells were washed twice with PBS and fixed by adding paraformaldehyde for 20 min. Wash 3 times with PBS, add 0.1% Triton X-100 soaked for 10 min, wash once with PBS, add goat serum closed at room temperature for 30 min, wash once with PBS, add primary antibody and incubate at 4°C overnight. Wash with PBS for 3 times, add fluorescent secondary antibody under light-avoidance condition, incubate for 1 h at room temperature, wash with PBS for 3 times, and add DAPI to stain the cell nuclear for 5 min, which can be observed and recorded under the inverted fluorescence microscope.

Immunohistochemistry: The synovial tissue was paraffin-embedded and sectioned, left to stand at 60°C for 30 min, deparaffinised by xylene, and placed in anhydrous ethanol for 3 minx3 times, 90%, 80% and 70% ethanol in that order, each for 3 min. Antigen repair was performed by placing in sodium citrate buffer (PH=6) and incubated for 10 min at room temperature with endogenous peroxidase blocker. Wash 3 times with PBS, add 5% goat serum with 0.1% Triton X-100 and incubate overnight at 4°C , add primary antibody, incubate overnight at 4°C , wash 3 times with PBS, add secondary antibody and incubate for 1 h at room temperature, Wash 3 times with PBS, add

DAB chromogenic solution and incubate at room temperature for 10 min, shake off the water, add hematoxylin to stain the nucleus for 2 min, dehydrate, clear, seal the film, observe and record under the microscope.

Statistical analysis

Data are presented as the means \pm standard deviation. An unpaired Student's T test was used to compare 2 groups. One-way analysis of variance was used for comparisons of more than 2 groups. When ANOVA showed statistical significance, a post-hoc test was subsequently performed. In this study, we used Tukey's honest significant difference test to test the two groups that were significantly different. P values <0.05 were considered statistically significant.

Results

RNA sequencing process and library construction

The RNA transcriptome is designed to quantify all RNA transcribed from a specific tissue or cell in a particular state and is based on the Illumina sequencing platform. Due to its high throughput, high sensitivity, and broad range of applications, the RNA transcriptome is extensively utilized in femoral head necrosis research. This study aimed to investigate the bioinformatics molecular markers of the "peri-collapsed" synovium in SIONFH by utilizing RNA sequencing of both synovial tissues and fibroblasts, the primary components of the synovial membrane. The objective of this study is to identify marker genes for the "peri-collapse" synovium in SIONFH, explore the molecular functions of these genes

through subsequent experiments, and ultimately inform clinical treatment. Samples were extracted using standard methods for quality control and library construction (Fig. 1).

RNA sequencing of SIONFH, FNF, and HOA hip synovium

Based on the gene expression profiles among different samples, the samples were subjected to expression distribution analysis, correlation analysis, and principal component analysis (PCA), as illustrated in Fig. 2A and B. The results indicated consistency among samples within each group, and the data displayed good quality and reproducibility, demonstrating significant variations among the different samples. Subsequently, a histogram was generated to illustrate the number of upregulated and downregulated differential genes across the various samples after comparison, as depicted in Fig. 2C. A total of 53 genes were identified as upregulated and 48 as downregulated in the HOA hip synovium compared to the FNF group. In comparison to the FNF group, 820 genes were upregulated and 286 downregulated in the SIONFH hip synovium, while 328 genes were upregulated and 79 downregulated when compared to the HOA group. The thresholds for differential gene screening were established as follows: P-value <0.05 , Fold Change (FC) ≥ 1.5 or FC ≤ -1.5 , and Variable Importance in the Projection (VIP, OPLS-DA) >1 .

Subsequently, a cluster analysis of gene expression was conducted to group and categorize the data based on similarity. In the clustering heatmap, closer clustering dendrites indicate a higher similarity in expression

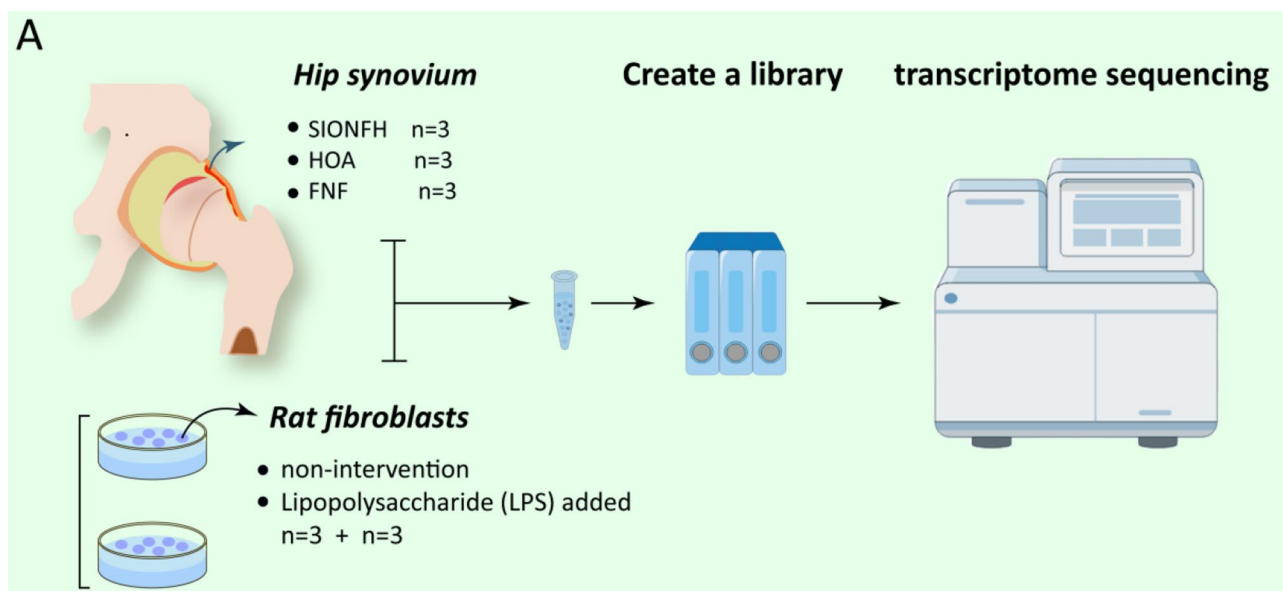


Fig. 1 Schematic of RNA sequencing. In order for the results to be statistically significant, SIONFH hip synovium ($n=3$), FNF hip synovium ($n=3$), HOA hip synovium ($n=3$), lipopolysaccharide-treated rat fibroblasts for 48 h ($n=3$) and untreated cells ($n=3$) were selected for RNA sequencing. This was followed by quality control, library construction and sequencing

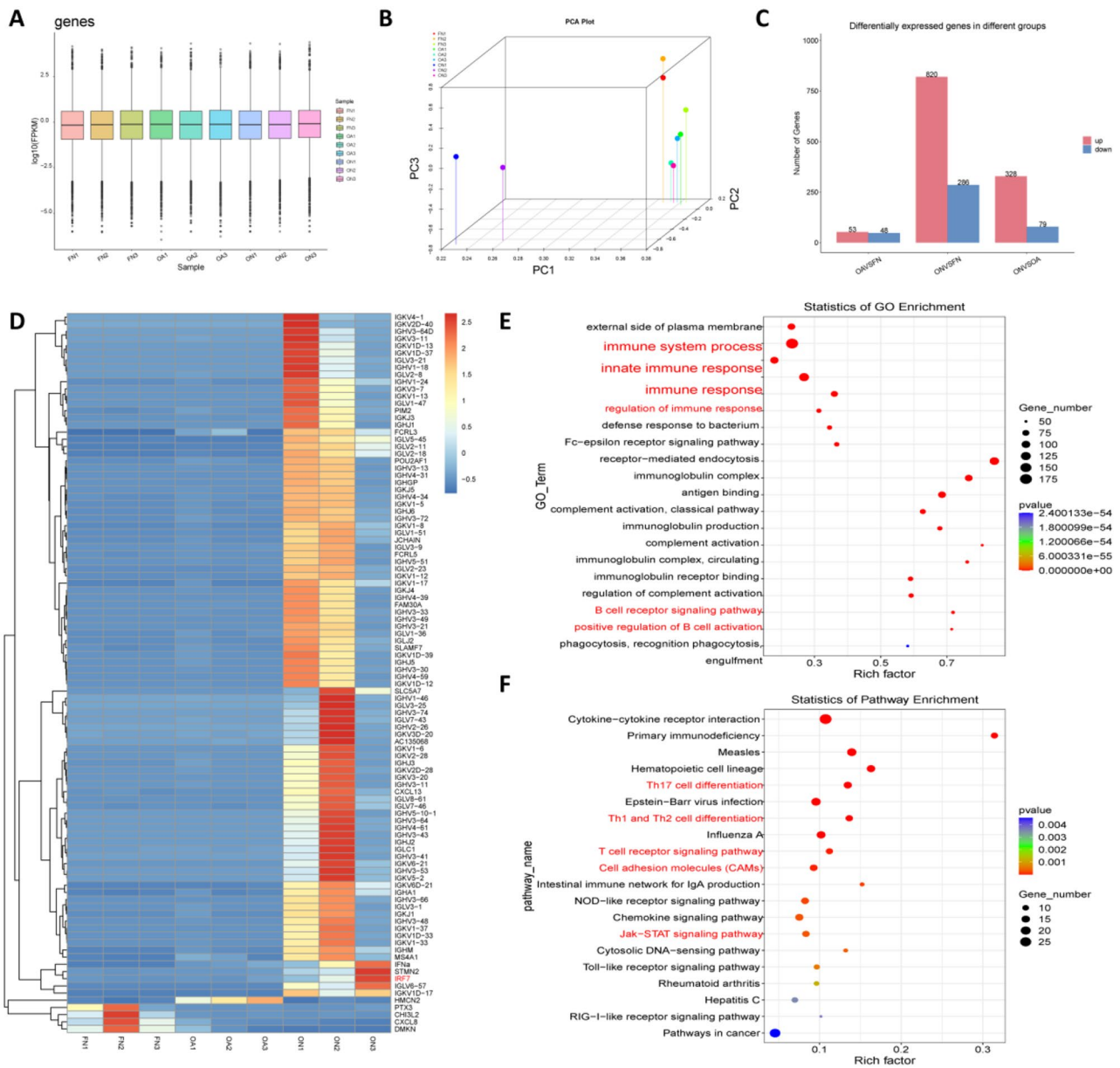


Fig. 2 Hip synovial tissue RNA sequencing quality control and results. **[A]** Gene expression boxplot reaction consistency of 9 samples. The results showed that all samples were in good agreement. **[B]** The PCA clustering results of 9 samples showed that the intra-group differences of samples in FNF, HOA and SIONFH groups were small, and the inter-group differences between SIONFH and FNF and HOA groups were large. **[C]** The number of up- and down-regulated genes in HOA vs. FNF, SIONFH vs. FNF, and SIONFH vs. HOA groups compared. Red color represents the number of up-regulated genes and blue color represents the number of down-regulated genes. **[D]** Heatmap of differential genes from RNA sequencing of synovial tissues of SIONFH, HOA, and FNF groups showed that IRF7, IFN α , and IG (immunoglobulin) family genes were significantly highly expressed in the synovial tissues of SIONFH ($P < 0.05$). HMCN2 was significantly highly expressed in the synovial tissues of HOA ($P < 0.05$). genes such as CHI3L2, DMKN, and other genes were significantly highly expressed in the synovial tissues of SIONFH. FNF synovial tissues ($P < 0.05$). **[E]** GO enrichment analysis of SIONFH vs. FNF vs. HOA differential genes showed that the differential genes in SIONFH synovium were mainly enriched in the process of immune system, innate immune response, regulation of immune response, B-cell receptor signaling pathway, and positive regulation of B-cell activation, etc. The results showed that SIONFH synovium had a high level of expression of CHI3L2, DMKN and other genes ($P < 0.05$). **[F]** KEGG enrichment of SIONFH vs. FNF vs. HOA differential genes showed that SIONFH differential genes were enriched in Th17 cell differentiation, Th1 and Th2 cell differentiation, T-cell receptor signaling pathway, cell adhesion molecules (CAMs), and Jak-STAT signaling pathway

patterns; redder colors represent higher relative expression, while bluer colors indicate lower relative expression. The clustering distance method utilized was “Euclidean distance”, and the clustering technique employed was “COMPLETE” linkage. The analysis revealed distinct gene expression patterns among the three groups of samples, with a significant elevation in the expression of the immunoglobulin (IG) gene family in the synovial membrane of the hip joints affected by SIONFH. Additionally, there was a notable increase in the expression of MS4A1, IFN α , STMN2, and IRF7. Notably, HMCN2 exhibited high expression in the HOA hip synovium, while PTX3, CHI3L2, and DMKN showed elevated expression levels in the FNF hip synovium.

Subsequently, pairwise comparisons were conducted among the three sets of samples. Transcriptome sequencing of the tissues revealed that the synovium of the hip joint affected by steroid-induced osteonecrosis of the femoral head exhibited high expression of 820 differentially expressed genes, which were primarily enriched in the extracellular space, adaptive immune response, defense response to bacteria, receptor-mediated endocytosis, leukocyte migration, complement activation, and other biological processes relevant to the femoral head, when compared to femoral neck fractures. Several pathways were identified, influencing cytokine-receptor interactions, chemokine signaling pathways, cell adhesion molecules, T cell receptor signaling pathways, and natural killer cell-mediated cytotoxicity. In comparison to hip osteoarthritis, steroid-induced osteonecrosis of the femoral head is associated with elevated synovial expression of 328 genes, which mediate biological processes primarily involving the external side of the plasma membrane, immune system processes, leukocyte migration, extracellular space, and adaptive immune responses. The relevant signaling pathways primarily include cytokine-receptor interactions, T-cell receptor signaling pathways, the NF-kappa B signaling pathway, and the Jak-STAT signaling pathway, among others. Finally, a comprehensive comparison of the results from the three groups of samples was performed, revealing significant enrichment in Gene Ontology (GO) entries related to immune system processes, innate immune responses, immune response modulation, B-cell receptor signaling pathways, as well as KEGG pathways associated with Th17 cell differentiation, Th1 and Th2 cell differentiation, T-cell receptor signaling pathways, cell adhesion molecules (CAM), and Jak-STAT signaling pathways.

HOOK1, RNPC3, KCNA3, CD48, IRF7, and SAMD9 are significantly overexpressed in the synovium of the hip joint in the “peri-collapse phase” of SIONFH

Fibroblasts are the predominant cell type in synovial tissue. Therefore, we treated them with 5 μ g/ml

lipopolysaccharide and performed RNA sequencing; the results are presented in Fig. 3. Transcriptomic analysis revealed that lipopolysaccharide-treated fibroblasts exhibited high expression of 893 differentially expressed genes compared to untreated fibroblasts. First, the consistency of the samples was assessed, and the results from the correlation plots indicated that the samples demonstrated good consistency. Next, the differential genes of lipopolysaccharide-treated fibroblasts were analyzed. The results from the volcano plot presented in Fig. 3B indicated that *Irf7*, *Vcam1*, *Ube2k*, *Phb*, *Fermt2*, *Iikap*, *Arl3*, *Traf6*, *Swt1*, and *Dcaf8* were significantly upregulated in the lipopolysaccharide group. Conversely, *Calm2*, *Sil1*, *Smc6*, *Trmt10c*, *Scarf2*, *Wdr81*, *Cmas*, *Dpm3*, *Tlr4*, and *Mfsd9* were significantly downregulated in the lipopolysaccharide-treated group. Differential gene enrichment analysis revealed significant enrichment in Gene Ontology (GO) entries related to negative regulation of the cell cycle, translation initiation factor activity, condensed chromosome kinetochore vesicles, endosomal components, regulation of DNA metabolic processes, Golgi vesicle transport, DNA repair, translational initiation, and other relevant processes, as illustrated in Fig. 3C.

The heatmap of differential gene expression presented in Fig. 3D indicates that *Irf7*, *Tph1*, *Calcl*, and *Spsb2* were significantly upregulated in the lipopolysaccharide group, while *Rcan2*, *Rps9*, and *Apln* were significantly downregulated. Gene Set Enrichment Analysis (GSEA) is not restricted to differential genes; it also elucidates whether a signaling pathway is repressed or activated. The results indicated that the primary enriched gene sets were associated with the necroptotic process, programmed necrotic cell death, protein targeting to the vacuole, JAK-STAT signaling pathway, NF- κ B signaling pathway, Nod-like receptor signaling pathway, TGF- β signaling pathway, TNF signaling pathway, and other relevant biological processes. The Venn diagram depicted in Fig. 3F illustrates the identification of six differentially expressed genes: *Hook1*, *Rnpc3*, *Kcna3*, *Cd48*, *Irf7*, and *Samd9*. The differential expression of these six genes, as presented in the RNA sequencing results in Fig. 3G, demonstrates that *Hook1*, *Rnpc3*, *Kcna3*, *Cd48*, *Irf7*, and *Samd9* were significantly upregulated in both the synovial membrane of the SIONFH hip joints ($P < 0.05$) and in lipopolysaccharide-treated fibroblasts ($P < 0.05$).

LPS significantly up-regulated the expression of *Irf7*, *Hook1*, *Rnpc3*, *Cd48*, *Samd9*, *Kcna3* in fibroblasts

To further validate the aforementioned results, *in vitro* experiments were conducted on fibroblasts. The fibroblasts were divided into a control group and a 5 μ g/ml LPS-treated group, and gene expression was verified by PCR on days 1, 2, and 3, respectively. The differences between the control group and the LPS-treated group

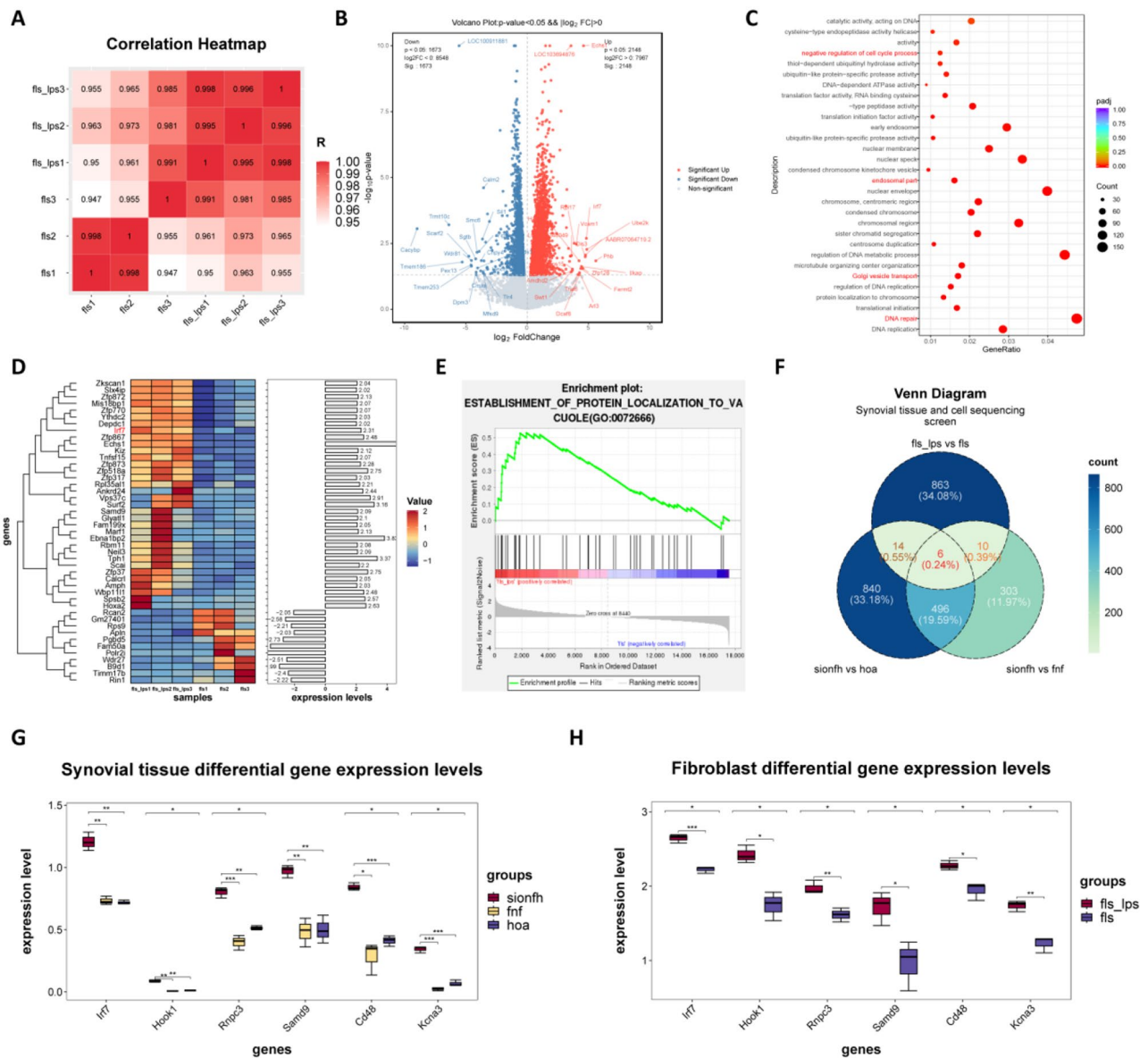


Fig. 3 Figure 3 HOOK1, RNPC3, KCNA3, CD48, IRF7, and SAMD9 are highly expressed in SIONFH synovium during the “peri-collapse phase”. [A] Heatmap of correlation coefficients of RNA sequencing samples from 5ug/ml lipopolysaccharide-treated fibroblasts (the higher the correlation coefficient between the samples, the closer their expression patterns). The results showed that the consistency of the samples in the lipopolysaccharide intervention group was better, and the fibroblast control group sample 3 was more different from samples 1 and 2, but the subsequent analysis was still performed considering its value of 0.947, which is close to 1. [B] Volcano plot of differential genes from RNA sequencing of fibroblasts, red represents up-regulated differential genes in lipopolysaccharide-treated fibroblasts and blue represents down-regulated differential genes. (P -value < 0.05 and $|\log_2 FC| > 1.5$). [C] Bubble plots of GO enrichment results for differential genes in lipopolysaccharide-treated fibroblasts showing enrichment in negative regulation of cell cycle process, endosomal part, Golgi vesicle transport, DNA repair. [D] Heatmap of RNA sequencing differential genes in lipopolysaccharide-treated fibroblasts showing *Irf7*, *Tph1*, *Calcr1*, *Spsb2* are highly expressed in the lipopolysaccharide-treated group, and genes such as *Rcan2*, *Rps9*, and *Apln* are lowly expressed in the lipopolysaccharide-treated group. Dendrograms of correlation are shown on the left, and histograms of fold difference are shown on the right. [E] GSEA plot of RNA sequencing enrichment analysis of lipopolysaccharide-treated fibroblasts, which showed significant enrichment in the ESTABLISHMENT OF PROTEIN LOCALIZATION TO VACUOLE entry. This suggests that protein transport and translocation may play a key role. [F] Venn diagram of RNA sequencing of SIONFH hip synovial tissue with RNA sequencing of differential genes in lipopolysaccharide-treated fibroblasts. Six differential genes were finally screened, namely HOOK1, RNPC3, KCNA3, CD48, IRF7, and SAMD9. [G] Differential expression of HOOK1, RNPC3, KCNA3, CD48, IRF7, and SAMD9 in synovial tissues of hip joints (Note: * indicates $P < 0.05$; ** indicates $P < 0.01$; *** indicates $P < 0.001$). Different colors represent different samples. [H] Differential expression of Hook1, Rnpc3, Kcna3, Cd48, Irf7, and Samd9 in RNA sequencing of lipopolysaccharide-treated fibroblasts (Note: * indicates $P < 0.05$; ** indicates $P < 0.01$; *** indicates $P < 0.001$). Different colors represent different samples

were analyzed on days 1, 2, and 3. The statistical differences are presented in Fig. 4. The results indicated that the expression of *Irf7*, *Hook1*, *Rnpc3*, *Cd48*, *Samd9*, and *Kcna3* was elevated on the first day of LPS treatment, with expression levels increasing over the duration of the intervention. This finding suggests that gene expression may be time-dependent, reaching its peak on the third day.

Il-6, *Tnfa* significantly downregulated in fibroblasts knocked down for *Irf7*

In the previous section, six genes were screened via RNA sequencing, specifically *IRF7*, *HOOK1*, *RNPC3*, *CD48*, *SAMD9*, and *KCNA3*. To elucidate the role of *IRF7* in the “peri-collapse phase” of SIONFH, lentiviral transfection was performed on fibroblasts to specifically knock down the expression of *Irf7*. Following experimental validation, the conditions for lentiviral transfection were optimized: a MOL concentration of 50, the inclusion of the co-transfection reagent HitransG P, and the addition of 2 $\mu\text{g}/\text{ml}$ puromycin for the selection of successfully transfected cells.

To characterize the efficiency of *Irf7* knockdown and its downstream molecular pathways, RT-qPCR and Western blot experiments were conducted. The experiments were divided into four groups: a fibroblast control group, a 5 $\mu\text{g}/\text{ml}$ lipopolysaccharide treatment group, an shRNA-*Irf7* transfection group, and an shRNA-control transfection group. Cells were cultured at 37 $^{\circ}\text{C}$ in a 5% CO_2 atmosphere for 1, 2, and 3 days for PCR and Western blot validation, respectively. *IRF7* is a key transcriptional regulator of type I interferon (IFN)-dependent immune responses and plays a critical role in the innate immune response against DNA and RNA viruses [36, 37]. To explore the inflammation-related pathways, the mRNA and protein expression levels of *Il-6* and *Tnfa* were also examined. The results indicated that the knockdown rate of *Irf7* was 71.1%, and the expression levels of *Il-6* and *Tnfa* significantly increased after lipopolysaccharide treatment in a time-dependent manner, peaking on day 3. Notably, the results also demonstrated that *Il-6* and *Tnfa* were closely associated with *Irf7*, with their expression levels significantly downregulated in the shRNA-*Irf7* group compared to the shRNA-control group. This

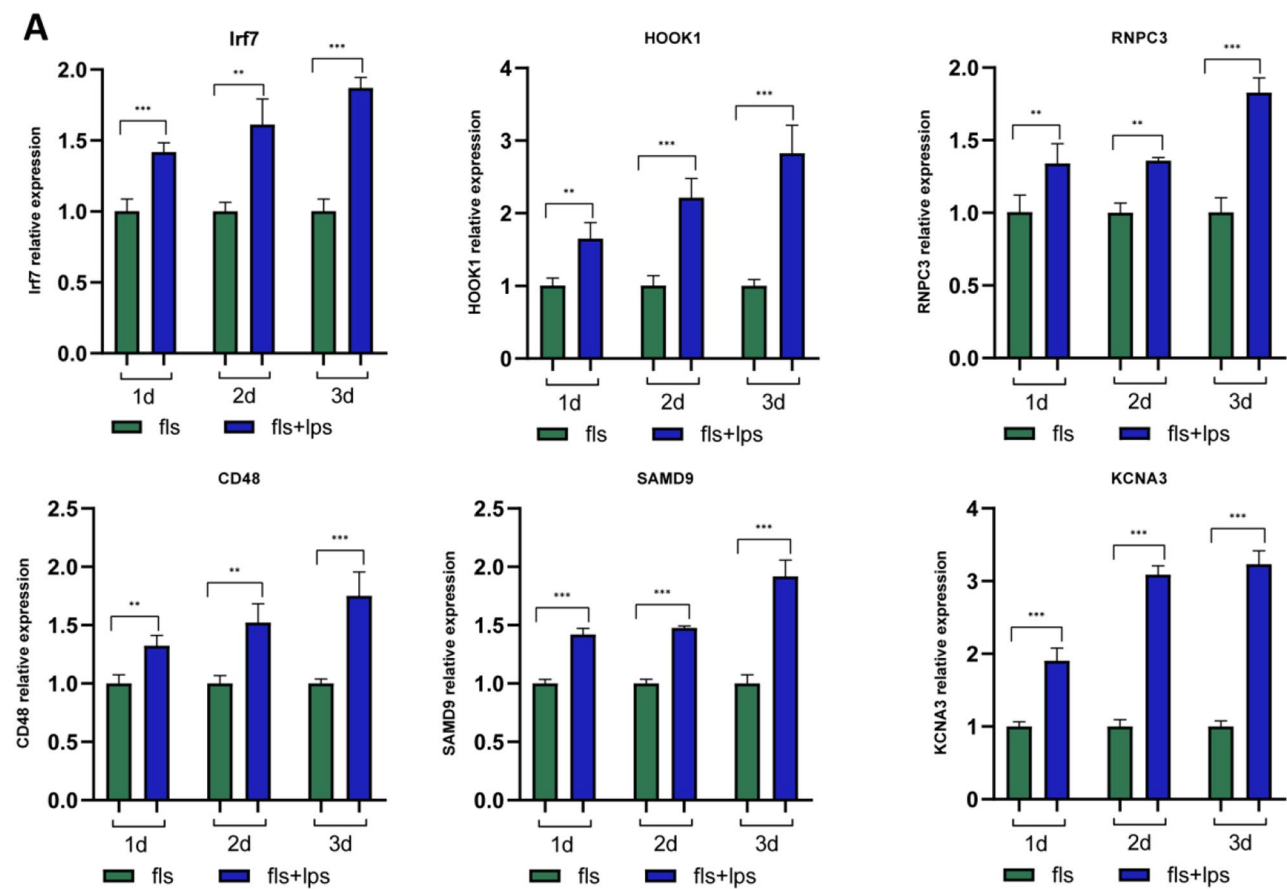


Fig. 4 In vitro experiments showed that LPS significantly up-regulated the expression of *Irf7*, *Hook1*, *Rnpc3*, *Cd48*, *Samd9*, *Kcna3* in fibroblasts. The experiments included a fibroblast control group and a 5 $\mu\text{g}/\text{ml}$ LPS intervention group, and the cells were collected on days 1, 2, 3 for PCR validation, respectively. (Note: * indicates $P < 0.05$; ** indicates $P < 0.01$; *** indicates $P < 0.001$). Significance analysis was performed using Independent Samples t-Test

suggests that *Irf7* mediates the activation of the *Il-6* and *Tnfa*-related pathways, playing a regulatory role in inflammation. The results of the Western blot experiment also supported this conclusion (Fig. 5).

Knockdown of *Irf7* inhibits the level of cell migration in fibroblasts

To evaluate the efficiency of lentiviral knockdown of *Irf7*, immunofluorescence experiments (IF) were performed. The experiment was divided into four groups: a fibroblast control group, a 5 µg/ml lipopolysaccharide treatment group, an shRNA-*Irf7* transfection group, and an shRNA-control transfection group. Cells were cultured at 37 °C in a 5% CO₂ atmosphere for 48 h for immunofluorescence experiments. The results of the immunofluorescence experiments indicated that lipopolysaccharide treatment significantly increased the expression of the *Irf7* gene, whereas the expression of *Irf7* protein was significantly downregulated in the shRNA-*Irf7* transfected

group. This finding suggests that the lentiviral transfection achieved a higher knockdown efficiency.

Cell migration capacity reflects the ability of inflammatory cells and factors to undergo chemotaxis [38]. Activation of fibroblast-like synoviocytes (FLS) is characterized by increased aggressiveness, akin to the distant metastasis of lymphocytes and tumor cells. This pathological process can lead to disease progression as FLS release inflammatory cytokines within the joints, subsequently recruiting additional FLS to undergo synovial proliferative reactions and invade the articular cartilage. Cell migration experiments demonstrated that lipopolysaccharide intervention significantly enhanced the ability of fibroblasts to migrate from the upper to lower layers of transwell chambers. This suggests that inflammatory stimulation promotes the biological expression of the inflammatory response in fibroblasts. Notably, the promotion of fibroblast migration was significantly suppressed following the knockdown of the *Irf7* gene,

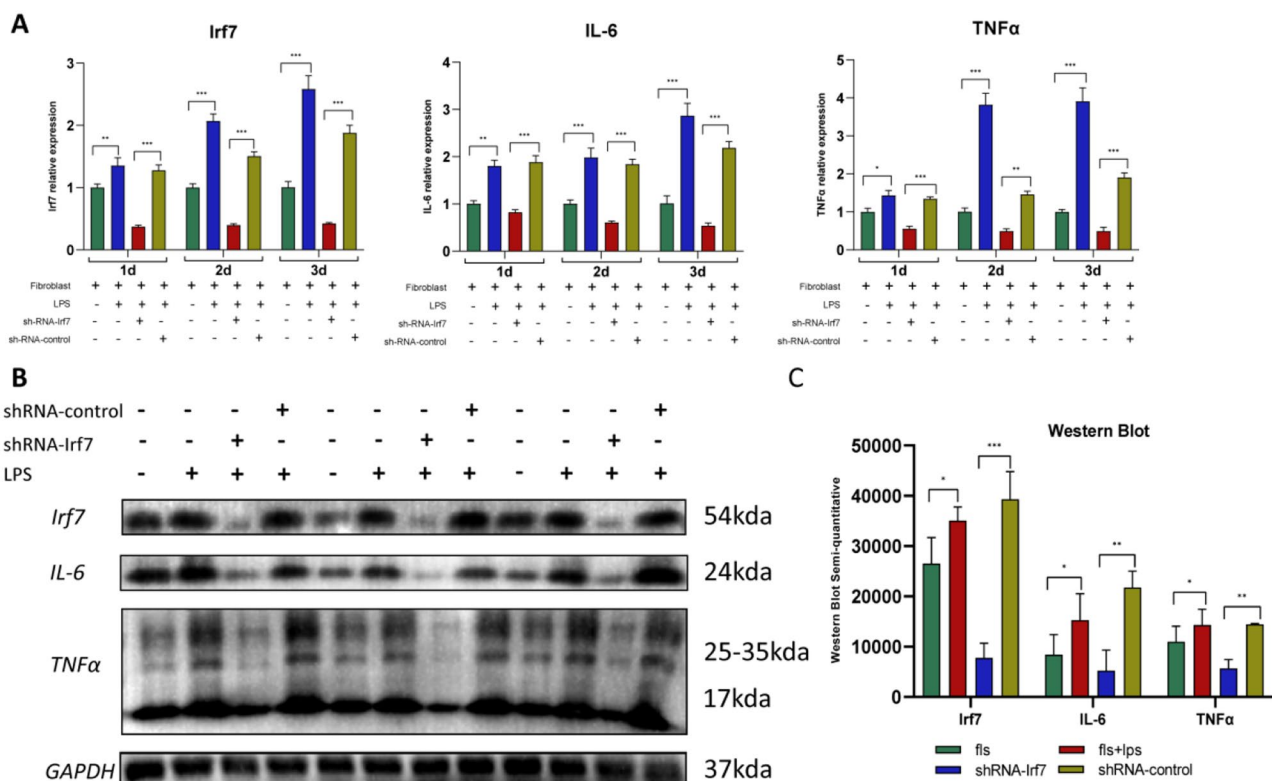


Fig. 5 *Il-6*, *Tnfa* significantly downregulated in fibroblasts knocked down for *Irf7*. **[A]** To verify the efficiency of lentiviral transfection to knockdown *Irf7*, we performed RT-qPCR experiments. The experiment was divided into four groups, fibroblast control group, 5µg/ml lipopolysaccharide treatment group, shRNA-*Irf7* transfection group, and shRNA-control transfection group. Cells in each group were cultured at 37 °C under 5% CO₂ for 1,2,3 days, after which PCR experiments were performed for verification. In addition, in order to explore the downstream genes of *Irf7*, we also detected *Il-6*, *Tnfa* by PCR experiments. (Note: One-way ANOVA was used for multiple comparisons; * indicates *P* < 0.05; ** indicates *P* < 0.01; *** indicates *P* < 0.001). **[B]** To verify the expression of relevant proteins after knockdown of *Irf7*, we performed Western Blot experiments. The experimental grouping was as above. We examined the expression of *Irf7*, *Il-6*, *Tnfa* proteins, the experiment was set up with 3 groups of replicates, and the protein molecular weights were labeled on the right side of the bands. **[C]** In order to quantitatively represent the expression of *Irf7*, *Il-6*, *Tnfa* proteins, we semi-quantitatively analyzed the bands and performed statistical plots. (Note: * indicates *P* < 0.05; ** indicates *P* < 0.01)

indicating that Irf7 is associated with the migratory capacity of fibroblasts (Fig. 6).

Synovitis manifestations are more prominent in the SIONFH hip synovium

To clarify the level of synovial inflammation in both the animal model of SIONFH and in patients, we developed a rat model of SIONFH [39] and collected the synovium from the hip joint for hematoxylin and eosin (HE) staining. The results indicated that in the animal specimens, the synovium of the hip joint in SIONFH rats exhibited a higher recruitment of inflammatory cells at the synovial rim, although no significant differences in histomorphology were observed. In human specimens, the FNF synovium displayed a softer morphology with no evidence of inflammatory cell recruitment. However,

both HOA and SIONFH exhibited synovial hyperplasia, structural disorganization, and extensive recruitment of inflammatory cells; notably, synovial inflammation was more pronounced in SIONFH. These findings suggest that the release of inflammatory factors in the femoral head during the peri-collapse and collapse phases of SIONFH contributes to synovial inflammation Fig. (7).

IRF7 is significantly overexpressed in the synovium of SIONFH hip joints

RNA sequencing results indicated that IRE7 was highly expressed in the hip synovium of SIONFH patients. Both immunohistochemistry (IHC) and immunofluorescence (IF) are capable of detecting the expression of relevant proteins in tissues. Immunohistochemistry (IHC) is a staining technique that employs the principle of specific

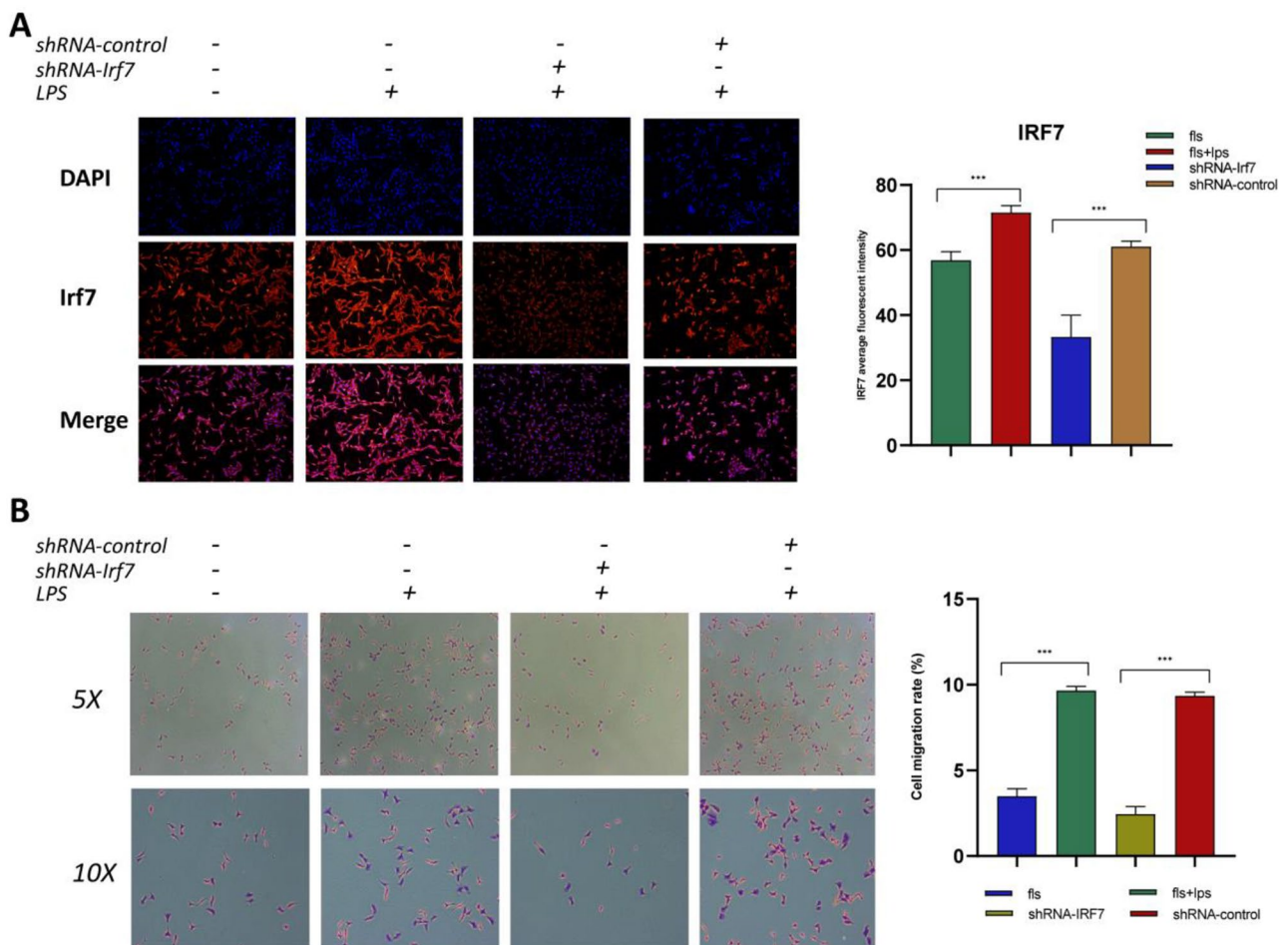


Fig. 6 Knockdown of Irf7 inhibits the level of cell migration in fibroblasts. **[A]** To verify the expression level of Irf7 gene after lentiviral transfection, we performed immunofluorescence (IF) experiments. The experiment was divided into four groups, namely, fibroblast control group, 5ug/ml lipopolysaccharide treatment group, shRNA-Irf7 group, and shRNA-control group. Cells were cultured at 37 °C under 5% CO₂ for 48 h for IF experiments. In order to quantitatively analyze the efficiency of knockdown of Irf7, we semi-quantitatively analyzed the IF results. (Note: One-way ANOVA was used for multiple samples; ** indicates $P < 0.01$; *** indicates $P < 0.001$). **[B]** To detect the migratory ability of fibroblasts, we performed experiments and stained with crystal violet. The experimental grouping was as above. The experimental method was to seed equal numbers of fibroblasts into the upper chamber of Transwell, and only serum-containing medium was added to the lower chamber. 48 h later, the fibroblasts in the lower chamber were subjected to crystal violet staining and the number of cells was counted. (Note: One-way ANOVA was used for multiple samples; *** indicates $P < 0.001$)

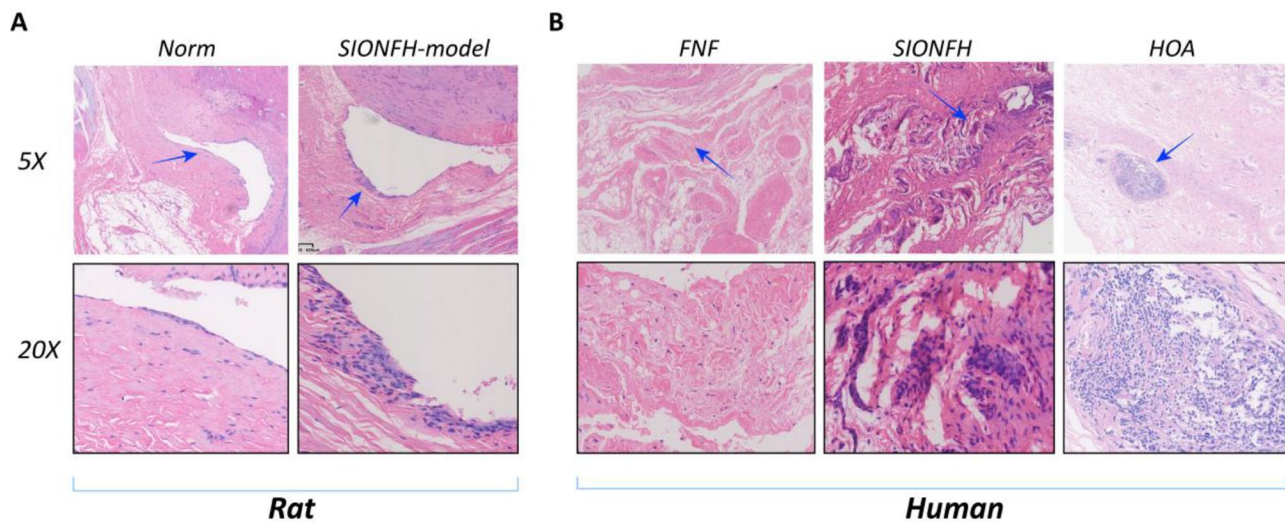


Fig. 7 Synovitis manifestations are more prominent in the SIONFH hip synovium. **[A]** To compare the level of synovitis in SIONFH disease, we built a SIONFH rat model and used HE staining to compare the level of inflammatory response in the synovium. Arrowheads stand in for magnified areas. **[B]** To compare the level of synovial inflammation in different diseases, we took hip synovium from femoral neck fracture (FNF), hip osteoarthritis (HOA), and hormonal osteonecrosis of the femoral head (SIONFH) for HE staining. Arrowheads stand in for magnified areas

antigen-antibody binding to characterize and localize antigenic substances in tissues or cells. Compared to other protein detection methods, IHC's primary advantages are its ability to characterize and localize antigenic substances accurately and its high qualitative sensitivity, establishing it as the preferred method for localization detection and analysis [40–42]. A significant advantage of immunofluorescence (IF) is its capability to label multiple proteins simultaneously, facilitating the determination of whether these proteins are co-expressed [43, 44]. In this study, vimentin (VIM) serves as a specific marker for synovial fibroblasts [45, 46], and the immunofluorescence double-staining assay of VIM and interferon regulatory factor 7 (Irf7) elucidates the abundance of Irf7 expression in synovial fibroblasts. In this study, we employed the immunohistochemistry (IHC) technique to investigate the localization of target proteins within the tissues and utilized the immunofluorescence (IF) technique to determine the co-expression of target proteins with Vimentin, the results are illustrated in Fig. 8. To further validate the expression level of IRF7, we conducted immunohistochemical (IHC) experiments on the hip synovium of SIONFH rats, as well as on that of FNE, HOA, and SIONFH patients. A darker coloration indicates a higher expression of the IRF7 protein. The results demonstrated that, compared to normal rats, the expression level of Irf7 protein was higher in the synovium of SIONFH rat hips. Interestingly, in the IHC experiments involving patients' hip synovium, IRF7 expression was significantly higher in the hip synovium of both HOA and SIONFH patients compared to FNF patients, with the highest expression observed in the SIONFH group. Subsequently, we performed fluorescence double-staining experiments for

VIM and IRF7 in the hip synovium of FNE, HOA, and SIONFH patients. In order to detect the expression of IRF7 in synovial tissues, the average fluorescence intensity was assessed using ImageJ software on the fluorescence result plots, and statistical analysis was performed. The results demonstrated that IRF7 expression was lowest in the FNF group and highest in the SIONFH group, with statistically significant differences observed. (Note: One-way ANOVA was employed for multiple group comparisons; statistical significance is indicated by *** ($P < 0.001$)).

IFN α downstream of IRF7 is significantly overexpressed in SIONFH hip synovium

Toll-like receptor (TLR) immunorecognition of virus-associated molecules triggers an intracellular signaling cascade, which subsequently activates interferon regulatory factors, particularly IRF7, leading to the expression of the type 1 interferon (IFN) gene family [36, 47]. Consequently, we characterized the expression of IFN α in the synovium of the SIONFH hip. In order to detect the differential expression of IFN α , immunohistochemistry (IHC) was conducted on the synovial tissues of the hip joints from human subjects diagnosed with SIONFH, FNE, HOA and in the SIONFH rat model. We also conducted fluorescence double staining experiments to assess IFN α and waveform proteins in the same human synovial tissues. In order to detect the expression of IFN α in synovial tissues, the average fluorescence intensity was assessed using ImageJ software on the fluorescence result plots, and statistical analysis was performed. The results indicated that IFN α expression was significantly elevated in the SIONFH-Rat group. Expression levels of

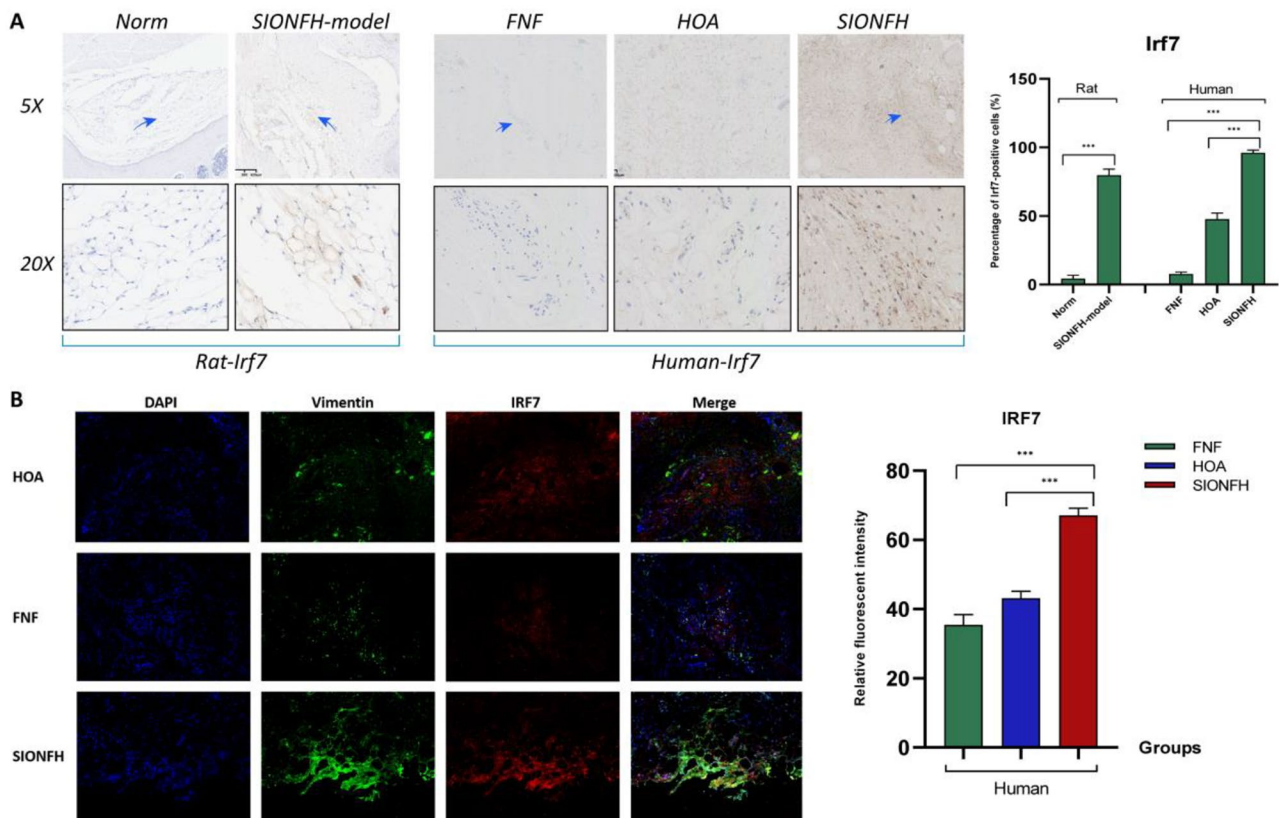


Fig. 8 IRF7 is significantly overexpressed in the synovium of SIONFH hip joints. **[A]** In order to clarify the expression of IRF7 in the synovium of SIONFH hips, we performed immunohistochemistry (IHC) experiments for IRF7 in the synovium of hips from SIONFH-Rat and in the synovium of hips from patients with FNF, HOA, and SIONFH. Arrowheads stand in for magnified areas, and we also counted and plotted the number of positive cells for IRF7. **[B]** Based on the above purpose, we also performed immunofluorescence (IF) experiments of IRF7 and VIM on the synovium of the hip joints of patients with FNF, HOA, and SIONFH, and we also statistically analyzed and graphed the average fluorescence intensity of the synovial samples of the three groups. (Note: One-way ANOVA was used for multiple group comparisons; *** indicates $P < 0.001$)

IFN α were lowest in the FNF group and highest in the SIONFH group, with the difference being statistically significant. Among the immunofluorescence results, IFN α exhibited the lowest expression in the FNF group and the highest in the SIONFH group, with a significant difference observed. These findings suggest that IFN α , downstream of IRF7, is significantly elevated in the synovium of SIONFH hips (Fig. 9).

Knockdown of Irf7 reverses synoviocyte-mediated chondrocyte apoptosis

To clarify the effect of SIONFH “peri-collapse” synovium on femoral head cartilage, we established an in vitro co-culture system of synovial fibroblasts and chondrocytes, as illustrated in Fig. 10A. The study included four experimental groups: a fibroblast control group, a 5 μ g/mL lipopolysaccharide treatment group, an shRNA-Irf7 transfection group, and an shRNA-control transfection group. Fibroblasts were initially treated for 48 h, after which they were transferred to the upper chamber of the co-culture system, while chondrocytes were placed in the lower chamber. Lipopolysaccharide was not introduced

during the co-culture to eliminate its effects on the chondrocytes in the lower chamber. Chondrocyte apoptosis indicators were assessed using RT-qPCR, Western blot analysis, and flow cytometry. The flow cytometry results presented in Fig. 10B indicate that fibroblasts in an inflammatory state (treated with lipopolysaccharide) enhanced the early apoptotic rate of chondrocytes, while the knockdown of Irf7 significantly mitigated this adverse effect. The results of RT-qPCR and Western blot analyses are presented in Fig. 10C and D. Notably, our findings revealed that the proliferation levels of chondrocytes (Col2a1, Aggrecan, Sox9) were significantly down-regulated, while the levels of cartilage matrix degradation (Mmp13) were notably up-regulated, and the apoptosis rate of chondrocytes was markedly increased in the lipopolysaccharide-treated fibroblast group. Furthermore, knockdown of Irf7 significantly reversed the effects of lipopolysaccharide. The results of the Western blot and RT-qPCR analyses collectively support this conclusion.

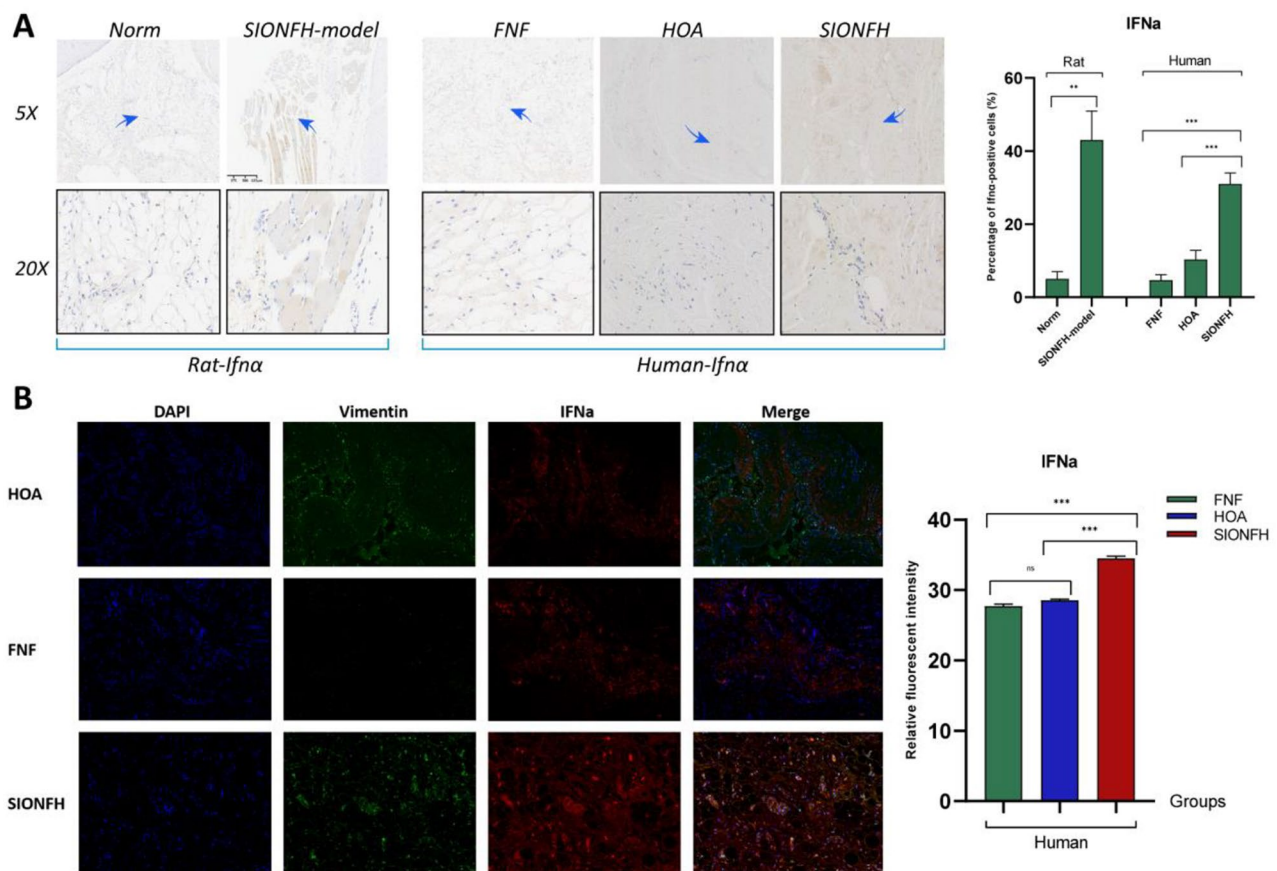


Fig. 9 IFN α downstream of IRF7 is significantly overexpressed in SIONFH hip synovium. **[A]** IFN α is a downstream protein of IRF7, therefore, we tested IFN α . As above, we performed IHC experiments for IFN α and counted and plotted the number of positive cells. (Note: One-way ANOVA was used for multiple comparisons; * indicates $P < 0.05$; *** indicates $P < 0.001$). **[B]** Similarly, we performed fluorescence double staining experiments of IFN α and VIM in the synovium of patients' hip joints, and the average fluorescence intensity was counted and plotted. (Note: One-way ANOVA was used for multiple group comparisons; *** indicates $P < 0.001$)

Discussions

In this study, we employed a comprehensive analysis of transcriptome sequencing across various sample types to refine the identification of SIONFH-associated differential genes, facilitating a more precise investigation of specific target genes. Compared to the FNF group, 820 differential genes were significantly upregulated in the synovium of SIONFH hips. In comparison to the HOA group, 328 genes were significantly upregulated in the synovium of SIONFH hips. The extensive number of differential genes hindered further mechanistic studies; therefore, we supplemented transcriptome sequencing of individual cells and ultimately identified six differential genes: HOOK1, RNPC3, KCNA3, CD48, IRF7, and SAMD9.

Cytoplasmic dynein facilitates the majority of minus-end-directed vesicular and organelle transport within the cell. Microtubules serve as polarized highways that facilitate the transport of organelles and vesicles throughout the cell. HOOK proteins are essential for early endosome trafficking [48]. Three HOOK isoforms are expressed in

humans: HOOK1, HOOK2, and HOOK3. Each isoform is associated with distinct cargo. HOOK3 localizes to the Golgi apparatus [49], HOOK2 is recruited to centrosomes [50], and HOOK1 is involved in endosomal transport [51, 52]. HOOK1 is primarily involved in the regulation of clathrin-independent endocytosis (CIE), a critical process for immune surveillance, cell migration, metastasis, and cell signaling [53, 54]. Our results demonstrated that HOOK1 is highly expressed in the synovium of SIONFH hips, suggesting enhanced intracellular vesicle and endosomal transport in synovial cells in SIONFH disease. This enhancement may be linked to the activation of inflammatory pathways as well as the exertion of anti-inflammatory effects. SAMD9 is recognized as a tumor suppressor that plays a significant role in various cancers and is involved in regulating cell proliferation, apoptosis, and the cell cycle by modulating several signaling pathways [55]. Furthermore, SAMD9 may also influence the pathogenesis of SIONFH.

Interferon regulatory factor 7 (IRF7) was originally identified as a master transcriptional factor responsible

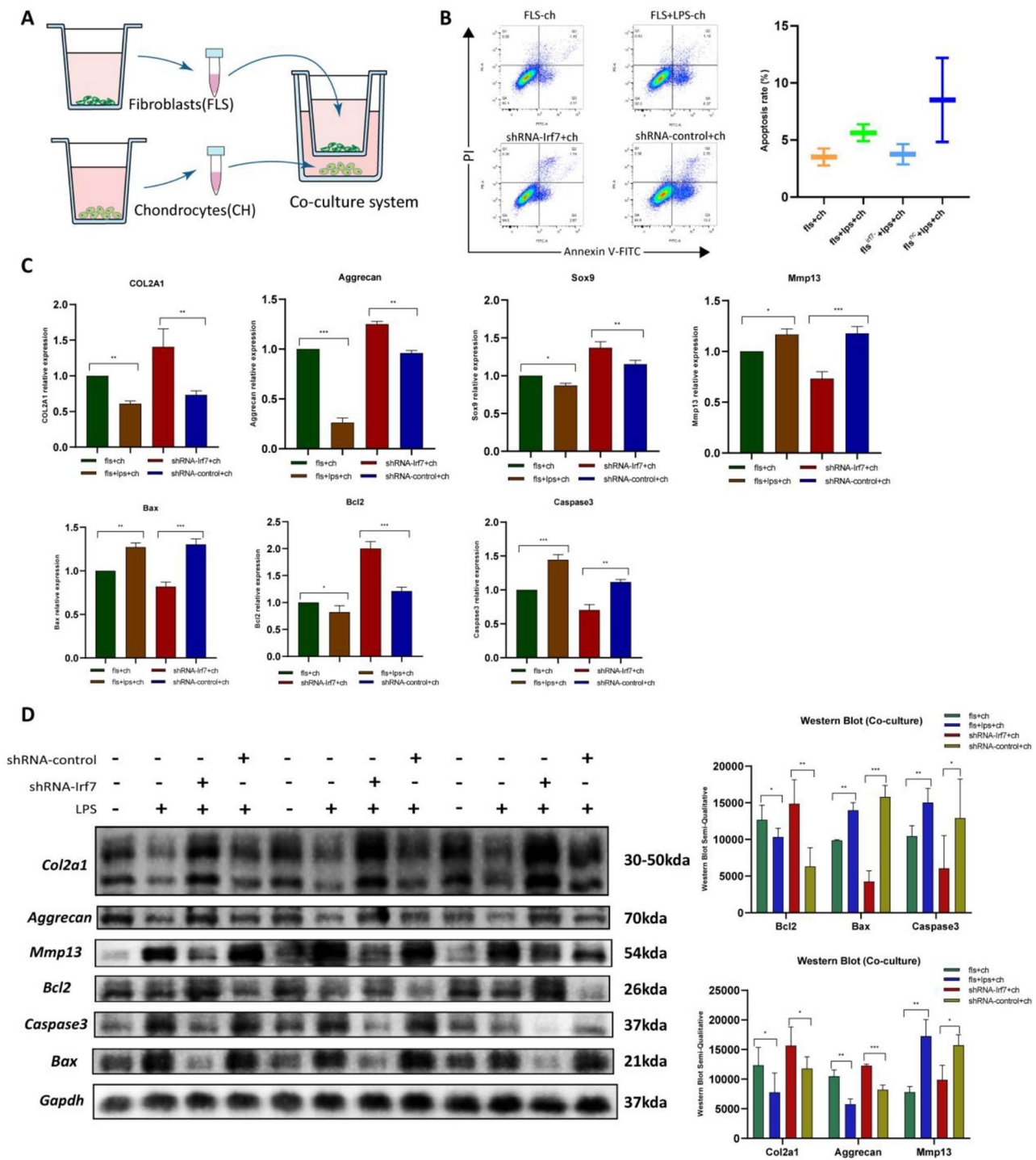


Fig. 10 (See legend on next page.)

for the production of type I interferon (IFN-I) and the regulation of the innate immune response. Subsequent studies have revealed that IRE7 performs multifaceted and versatile functions in various biological processes [56]. Interferon regulatory factors (IRFs) constitute a family of master transcription factors. Although IRFs

are acknowledged as transcriptional regulators of type I interferons (IFN-I) and IFN-inducible genes, this family is now characterized as key regulators in various processes, including immunity, oncogenesis, metabolism, cell differentiation, and apoptosis [57]. Dimerized IRE7 or an IRE3/IRE7 complex can translocate into the nucleus

(See figure on previous page.)

Fig. 10 Knockdown of *Irf7* reverses synoviocyte-mediated chondrocyte apoptosis. **[A]** To clarify the effect of synovial fibroblasts on chondrocytes, we established a cell co-culture device. It was divided into 4 groups, which were fibroblast control group, 5ug/ml lipopolysaccharide treatment group, shRNA-*Irf7* transfection group, and shRNA-control transfection group. The cells were pretreated for 48 h, after which they were transferred into the upper chamber of the co-culture system, and the chondrocytes were transferred into the lower chamber of the co-culture system, and cultured at 37°C with 5% CO₂ for 48 h, after which they were subjected to RT-qPCR, Western Blot, and flow cytometry. **[B]** To verify the effect of synovial fibroblasts on chondrocytes, we used flow cytometry for detecting the level of chondrocyte apoptosis. And the results were statistically analyzed and counted. **[C]** To verify the effect of synovial fibroblasts on mRNA expression of chondrocytes, we used RT-qPCR for detecting the mRNA expression level of chondrocyte *Col2a1*, *Aggrecan*, *Sox9*, *Mmp13*, *Bax*, *Bcl2*, and *Caspase3* indicators. Grouping as above. (Note: One-way ANOVA was used for multiple group comparisons; * indicates $P < 0.05$; ** indicates $P < 0.01$; *** indicates $P < 0.001$). **[D]** To verify the effect of synovial fibroblasts on chondrocyte apoptosis, we examined the protein expression of chondrocyte *Col2a1*, *Aggrecan*, *Mmp13*, *Bax*, *Bcl2*, *Caspase3*. The grouping was as above. In order to quantify the amount of expressed proteins, we used Image J software to analyze the bands semi-quantitatively, and performed statistical analysis and graphing. (The experiment was set up with 3 groups of replicates, and one-way ANOVA was used for multiple comparisons; * indicates $P < 0.05$; ** indicates $P < 0.01$; *** indicates $P < 0.001$)

to initiate the expression of the IFN-I gene. Furthermore, IRF7 is recognized as a susceptibility locus, with TRAP and *Gfil* preventing susceptibility to systemic lupus erythematosus (SLE) by regulating the nuclear transport of IRF7 [58]. Moreover, IRF7 has been associated with the pathogenesis of several autoimmune diseases, including multiple sclerosis [59], rheumatoid arthritis, systemic lupus erythematosus [60], systemic sclerosis [61], autoimmune pancreatitis, autoimmune thyroid diseases [62], and diabetes [63]. Glucocorticoids are considered essential therapeutic agents for autoimmune diseases. While our focus was on the synovial tissue of the femoral head affected by osteonecrosis due to glucocorticoids abuse, we did not investigate whether the patients had a history of autoimmune disease. Consequently, the link between the high expression of the IRF7 gene in the synovial membranes of SIONFH and the patients' history remains uncertain.

Our findings indicate that IFN signaling plays a causal role in host defense against infectious pathogens; its dysregulation is widely associated with autoimmune diseases, interferonopathies, infections, and cancer. As previously mentioned, IRF7 serves as the primary regulatory factor for IFN-I and IFN-III. Small molecules can influence the transcription, translation, post-translational regulation, and nuclear transport of IRF7, thereby regulating the production of interferons. Consequently, IRF7 is anticipated to serve as a promising therapeutic target for IFN-associated diseases. Additionally, we demonstrated in vitro that IRF7 is associated with the expression levels of IL-6 and TNF- α genes. In the co-culture system, lipopolysaccharide promotes the expression of the IRF7 gene in fibroblasts, leading to matrix degradation and apoptosis in chondrocytes. Moreover, following the knockdown of IRF7, the levels of matrix degradation and apoptosis in chondrocytes mediated by fibroblasts were significantly suppressed following the intervention of lipopolysaccharide, although not completely eliminated. This suggests that IRF7 plays a partial role in fibroblast-mediated apoptosis in chondrocytes, indicating that additional pathways beyond the IRF7 pathway are involved in this process.

Osteonecrosis of the femoral head (ONFH) is frequently attributed to glucocorticoids, which represent one of the most common non-traumatic causes. However, the pathogenesis of steroid-induced osteonecrosis of the femoral head (SIONFH) is highly complex and may be closely related to several mechanisms, including endothelial cell damage, coagulation abnormalities, and a tendency for thrombosis [64]; oxidative stress and reactive oxygen species mechanisms [65]; lipid metabolism disorders and fat embolism mechanisms [66]; mechanisms of apoptosis and autophagy [67]; and mechanisms of immune imbalance [68]. Currently, many researchers assert that the dynamic balance between bone formation and resorption constitutes a regulated inflammatory response, with various inflammatory cells and cytokines playing a crucial role in maintaining bone homeostasis [69]. A notable characteristic of SIONFH is the presence of an abnormal chronic inflammatory response. Under chronic inflammatory conditions, the effective reconstruction and repair of necrotic bone are impeded [70]. Patients with SIONFH undergoing total hip replacement surgery frequently exhibit inflamed synovial tissue upon gross examination at the time of surgery. Modulating immunity and restoring the balance of the immune system have positive implications for the treatment of SIONFH. For instance, Yinshi Ren et al. employed tocilizumab, an anti-IL-6 treatment, and found that the mean hip synovitis score, as well as the number of synovial macrophages and vessels, were significantly lower in the tocilizumab group compared to the no-treatment group. Additionally, tocilizumab anti-IL-6 treatment reduced hip synovitis and bone resorption while promoting new bone formation following ischemic osteonecrosis. This suggests that anti-inflammatory treatment reduces synovitis and enhances bone healing [71, 72].

In addition to synovial inflammation, glucocorticoid-induced osteonecrosis of the femoral head is closely associated with a local immune response characterized by abnormal macrophage activation and inflammatory cell infiltration at the necrotic site, resulting in a pro-inflammatory microenvironment dominated by M1 macrophages, ultimately leading to failure of bone repair

and regeneration [73]. Yue Luo et al. [74] report a bone regeneration strategy that involves the construction of an immune regulatory biomaterial platform utilizing an injectable thiolated hyaluronic acid hydrogel combined with lithium-doped nano-hydroxyapatite (Li-nHA@Gel) for the treatment of osteonecrosis. Li-nHA@Gel achieves sustained and long-term release of Li ions, which may enhance M2 macrophage polarization through activation of the JAK1/STAT6/STAT3 signaling pathway. The induced pro-repair immune microenvironment subsequently mediates the enhancement of osteogenic and angiogenic differentiation. Thus, therapeutic strategies aimed at modulating immune homeostasis in SIONFH hold great promise. Based on the results of this study, we identified elevated expression levels of IRF7 in the synovium of SIONFH and found that IRF7 plays a critical role in mediating the promotion of chondrocyte apoptosis by fibroblasts through gene silencing and co-culture techniques. In the next step, we will sequence fibroblasts with IRF7 knockdown to thoroughly evaluate the specific pathogenic mechanisms of IRF7 in the synovium of SIONFH patients. Therefore, anti-inflammatory therapy targeting IRF7 could represent a valuable therapeutic strategy.

Conclusions

In conclusion, transcriptome sequencing of human synovial tissue, along with transcriptome sequencing of lipopolysaccharide-treated fibroblasts, revealed a high expression profile of the genes HOOK1, RNPC3, KCNA3, CD48, IRF7, and SAMD9 in SIONFH. Downstream experiments demonstrated that IRF7 plays a critical role, potentially related to the activation of downstream inflammatory pathways in fibroblasts within the synovium and the induction of chondrocyte matrix degradation and apoptosis, establishing IRF7 as a potential target for delaying the progression of SIONFH collapse.

Supplementary Information

The online version contains supplementary material available at <https://doi.org/10.1186/s13018-025-0557-x>.

Supplementary Material 1

Acknowledgements

This work was supported by National Natural Science Foundation of China (82274544); National Natural Science Foundation of China Youth Science Foundation (82004392); Key Projects of Guangdong Provincial Administration of Traditional Chinese Medicine (20223012); NATCM's Project of High-level Construction of Key TCM Disciplines (Traditional Chinese Orthopedics); Traditional Chinese Orthopedics Open subject of FTSM (Grant number: XGS 2023008).

Author contributions

H LF, F WH contributed equally, are the co-first author of this paper; H ML participated in this experiment; Z ZK, H MC and W QS are the

co-corresponding author of this study; All authors contributed to manuscript revision, read, and approved the submitted version.

Funding

This work was supported by National Natural Science Foundation of China (82274544); National Natural Science Foundation of China Youth Science Foundation (82004392); Key Projects of Guangdong Provincial Administration of Traditional Chinese Medicine (20223012); NATCM's Project of High-level Construction of Key TCM Disciplines (Traditional Chinese Orthopedics); Traditional Chinese Orthopedics Open subject of FTSM (Grant number: XGS 2023008).

Data availability

No datasets were generated or analysed during the current study.

Declarations

Ethics approval and consent to participate

This study was approved by the board of research ethics in The Third Affiliated Hospital of Guangzhou University of Chinese Medicine (Approval No. PJ-XS-20230523-002). All patients give informed consent.

Consent for publication

All authors of this manuscript agree with the views expressed in this article and consent to publication.

Competing interests

The authors declare no competing interests.

Author details

¹Guangzhou University of Chinese Medicine, Guangdong 510405 Guangzhou, China

²Guangdong Academy of Traditional Chinese Medicine Orthopedics and Traumatology, Guangdong 510378 Guangzhou, China

³Joint Center of the Third Affiliated Hospital of Guangzhou University of Chinese Medicine, Guangdong 510378 Guangzhou, China

⁴Department of Orthopaedic Surgery, Quanzhou Orthopedic-traumatological Hospital, Quanzhou 362000, China

Received: 3 January 2025 / Accepted: 31 January 2025

Published online: 18 March 2025

References

1. Zhai S, Wu R, Zhao J, Huang W, Hu W, Huang W. Effectiveness of various interventions for non-traumatic osteonecrosis: a pairwise and network meta-analysis. *Front Endocrinol (Lausanne)*. 2024;15:1428125.
2. Chen Y, Miao Y, Liu K, Xue F, Zhu B, Zhang C, Li G. Evolutionary course of the femoral head osteonecrosis: histopathological - radiologic characteristics and clinical staging systems. *J Orthop Translat*. 2022;32:28–40.
3. Sun H, Zhang W, Yang N, Xue Y, Wang T, Wang H, Zheng K, Wang Y, Zhu F, Yang H, Xu W, Xu Y, Geng D. Activation of cannabinoid receptor 2 alleviates glucocorticoid-induced osteonecrosis of femoral head with osteogenesis and maintenance of blood supply. *Cell Death Dis*. 2021;12:1035.
4. Cui Q, Jo WL, Koo KH, Cheng EY, Drescher W, Goodman SB, Ha YC, Hernigou P, Jones LC, Kim SY, Lee KS, Lee MS, Lee YJ, Mont MA, Sugano N, Taliaferro J, Yamamoto T, Zhao D. Arco consensus on the pathogenesis of non-traumatic osteonecrosis of the femoral head. *J Korean Med Sci*. 2021;36:e65.
5. Zhang J, Cao J, Liu Y, Zhao H. Advances in the pathogenesis of steroid-associated osteonecrosis of the femoral head. *Biomolecules* 2024; 14.
6. Migliorini F, Maffulli N, Eschweiler J, Tingart M, Baroncini A. Core decompression isolated or combined with bone marrow-derived cell therapies for femoral head osteonecrosis. *Expert Opin Biol Ther*. 2021;21:423–30.
7. Sadile F, Bernasconi A, Russo S, Maffulli N. Core decompression versus other joint preserving treatments for osteonecrosis of the femoral head: a meta-analysis. *Br Med Bull*. 2016;118:33–49.
8. Migliorini F, La Padula G, Oliva F, Torsiello E, Hildebrand F, Maffulli N. Operative management of avascular necrosis of the femoral head in skeletally immature patients: a systematic review. *Life (Basel)* 2022; 12.

9. Quaranta M, Miranda L, Oliva F, Aletto C, Maffulli N. Osteotomies for avascular necrosis of the femoral head. *Br Med Bull*. 2021;137:98–111.
10. Migliorini F, Maffulli N, Baroncini A, Eschweiler J, Tingart M, Betsch M. Prognostic factors in the management of osteonecrosis of the femoral head: a systematic review. *Surgeon*. 2023;21:85–98.
11. Migliorini F, Maffulli N, Baroncini A, Eschweiler J, Tingart M, Betsch M. Failure and progression to total hip arthroplasty among the treatments for femoral head osteonecrosis: a bayesian network meta-analysis. *Br Med Bull*. 2021;138:112–25.
12. Ura H, Niida Y. Comparison of rna-sequencing methods for degraded rna. *Int J Mol Sci* 2024; 25.
13. Crossetto N, Bienko M, van Oudenaarden A. Spatially resolved transcriptomics and beyond. *Nat Rev Genet*. 2015;16:57–66.
14. Deng Z, Kim H, Hernandez PA, Ren Y. Fat phagocytosis promotes anti-inflammatory responses of macrophages in a mouse model of osteonecrosis. *Cells-Basel* 2024; 13.
15. Liu G, Luo S, Lei Y, Jiao M, Cao R, Guan H, Tian R, Wang K, Yang P. Osteogenesis-related long noncoding rna gas5 as a novel biomarker for osteonecrosis of femoral head. *Front Cell Dev Biol*. 2022;10:857612.
16. Li L, Ding Y, Liu B, Wang Z, Carlone DL, Yu X, Wei X, Zhang F, Lineaweaver WC, Yang B, Xia W, Wang DZ, Zhao D. Transcriptome landscape of the late-stage alcohol-induced osteonecrosis of the human femoral head. *Bone*. 2021;150:116012.
17. Kuang MJ, Zhang KH, Qiu J, Wang AB, Che WW, Li XM, Shi DL, Wang DC. Exosomal mir-365a-5p derived from huc-mscs regulates osteogenesis in gionfh through the hippo signaling pathway. *Mol Ther Nucleic Acids*. 2021;23:565–76.
18. Zuo W, Guo WS, Yu HC, Liu P, Zhang QD. Role of junction-mediating and regulatory protein in the pathogenesis of glucocorticoid-induced endothelial cell lesions. *Orthop Surg*. 2020;12:964–73.
19. Wei B, Wei W. Identification of aberrantly expressed of serum micrnas in patients with hormone-induced non-traumatic osteonecrosis of the femoral head. *Biomed Pharmacother*. 2015;75:191–5.
20. Yamaguchi R, Kamiya N, Adapala NS, Drissi H, Kim HK. Hif-1-dependent il-6 activation in articular chondrocytes initiating synovitis in femoral head ischemic osteonecrosis. *J Bone Joint Surg Am*. 2016;98:1122–31.
21. Kamiya N, Yamaguchi R, Adapala NS, Chen E, Neal D, Jack O, Thoveson A, Gudmundsson P, Brabham C, Aruwajoye O, Drissi H, Kim HK. Legg-calvé-perthes disease produces chronic hip synovitis and elevation of interleukin-6 in the synovial fluid. *J Bone Min Res*. 2015;30:1009–13.
22. Wei Qiushi HWZQ. Clinical significance of different imaging manifestations of osteonecrosis of femoralhead in the peri-collapse stage. *Zhong Guo Xiu Fu Chong Jian Wai Ke Za Zhi*. 2021;35:09:1105–1110.
23. Liu Yuhao ZCCL. A summary of hip-preservation surgery based on peri-collapse stage of osteonecrosis of femoral head. *Zhong Guo Xiu Fu Chong Jian Wai Ke Za Zhi*. 2017;31:08:1010–1015.
24. Rush BH, Bramson RT, Ogden JA. Legg-calvé-perthes disease: detection of cartilaginous and synovial change with mr imaging. *Radiology*. 1988;167:473–6.
25. Wingstrand H. Significance of synovitis in legg-calvé-perthes disease. *J Pediatr Orthop B*. 1999;8:156–60.
26. Sharma S, Tenoever BR, Grandvaux N, Zhou GP, Lin R, Hiscott J. Triggering the interferon antiviral response through an ikk-related pathway. *Science*. 2003;300:1148–51.
27. Honda K, Yanai H, Negishi H, Asagiri M, Sato M, Mizutani T, Shimada N, Ohba Y, Takaoka A, Yoshida N, Taniguchi T. Irf-7 is the master regulator of type-i interferon-dependent immune responses. *Nature*. 2005;434:772–7.
28. Kosukegawa I, Okazaki S, Yamamoto M, Nagoya S, Suzuki C, Shimizu J, Takahashi H, Yamashita T. The proton pump inhibitor, lansoprazole, prevents the development of non-traumatic osteonecrosis of the femoral head: an experimental and prospective clinical trial. *Eur J Orthop Surg Traumatol*. 2020;30:713–21.
29. Okazaki S, Nagoya S, Matsumoto H, Mizuo K, Sasaki M, Watanabe S, Yamashita T, Inoue H. Development of non-traumatic osteonecrosis of the femoral head requires toll-like receptor 7 and 9 stimulations and is boosted by repression on nuclear factor kappa b in rats. *Lab Invest*. 2015;95:92–9.
30. Meng K, Liu Y, Ruan L, Chen L, Chen Y, Liang Y. Suppression of apoptosis in osteocytes, the potential way of natural medicine in the treatment of osteonecrosis of the femoral head. *Biomed Pharmacother*. 2023;162:114403.
31. Fuchs Y, Steller H. Live to die another way: modes of programmed cell death and the signals emanating from dying cells. *Nat Rev Mol Cell Biol*. 2015;16:329–44.
32. Tao SC, Yuan T, Rui BY, Zhu ZZ, Guo SC, Zhang CQ. Exosomes derived from human platelet-rich plasma prevent apoptosis induced by glucocorticoid-associated endoplasmic reticulum stress in rat osteonecrosis of the femoral head via the akt/bad/bcl-2 signal pathway. *Theranostics*. 2017;7:733–50.
33. Lu X, Wu J, Qin Y, Liang J, Qian H, Song J, Qu C, Liu R. Identification of n-glycoproteins of hip cartilage in patients with osteonecrosis of femoral head using quantitative glycoproteomics. *Int J Biol Macromol*. 2021;187:892–902.
34. Yamamoto S, Watanabe A, Nakamura J, Ohtori S, Harada Y, Kishida S, Wada Y, Takahashi K. Quantitative t2 mapping of femoral head cartilage in systemic lupus erythematosus patients with noncollapsed osteonecrosis of the femoral head associated with corticosteroid therapy. *J Magn Reson Imaging*. 2011;34:1151–8.
35. Magnussen RA, Guilak F, Vail TP. Articular cartilage degeneration in post-collapse osteonecrosis of the femoral head. Radiographic staging, macroscopic grading, and histologic changes. *J Bone Joint Surg Am*. 2005;87:1272–7.
36. Génin P, Vaccaro A, Civas A. The role of differential expression of human interferon-a genes in antiviral immunity. *Cytokine Growth Factor Rev*. 2009;20:283–95.
37. Solis M, Goubau D, Romieu-Mourez R, Genin P, Civas A, Hiscott J. Distinct functions of irf-3 and irf-7 in ifn-alpha gene regulation and control of anti-tumor activity in primary macrophages. *Biochem Pharmacol*. 2006;72:1469–76.
38. Gerter R, Kruegel J, Miosge N. New insights into cartilage repair - the role of migratory progenitor cells in osteoarthritis. *Matrix Biol*. 2012;31:206–13.
39. Tian JQ, Wei TF, Wei YR, Xiao FJ, He XS, Lin K, Lu S, He XM, He W, Wei QS, Xiang XW, He MC. Effect of whole body vibration therapy in the rat model of steroid-induced osteonecrosis of the femoral head. *Front Cell Dev Biol*. 2023;11:1251634.
40. O'Leary TJ. Standardization in immunohistochemistry. *Appl Immunohistochem Mol Morphol*. 2001;9:3–8.
41. Rimm DL. Next-gen immunohistochemistry. *Nat Methods*. 2014;11:381–3.
42. Mckenney JK, Hornick JL. Immunohistochemistry in surgical pathology. *Adv Anat Pathol*. 2018;25:373.
43. Odell ID, Cook D. Immunofluorescence techniques. *J Invest Dermatol*. 2013;133:e4.
44. Ferri GL, Gaudio RM, Castello IF, Berger P, Giro G. Quadruple immunofluorescence: a direct visualization method. *J Histochem Cytochem*. 1997;45:155–8.
45. Maehira H, Miyake T, Iida H, Tokuda A, Mori H, Yasukawa D, Mukaisho KI, Shimizu T, Tani M. Vimentin expression in tumor microenvironment predicts survival in pancreatic ductal adenocarcinoma: heterogeneity in fibroblast population. *Ann Surg Oncol*. 2019;26:4791–804.
46. Strutz F, Okada H, Lo CW, Danoff T, Carone RL, Tomaszewski JE, Neilson EG. Identification and characterization of a fibroblast marker: fsp1. *J Cell Biol*. 1995;130:393–405.
47. Colonna M. Tlr pathways and ifn-regulatory factors: to each its own. *Eur J Immunol*. 2007;37:306–9.
48. Olenick MA, Tokito M, Boczkowska M, Dominguez R, Holzbaur EL. Hook adaptors induce unidirectional processive motility by enhancing the dynein-dynactin interaction. *J Biol Chem*. 2016;291:18239–51.
49. Walenta JH, Didier AJ, Liu X, Krämer H. The golgi-associated hook3 protein is a member of a novel family of microtubule-binding proteins. *J Cell Biol*. 2001;152:923–34.
50. Szebenyi G, Hall B, Yu R, Hashim AI, Krämer H. Hook2 localizes to the centrosome, binds directly to centriolin/cep110 and contributes to centrosomal function. *Traffic*. 2007;8:32–46.
51. Maldonado-Báez L, Cole NB, Krämer H, Donaldson JG. Microtubule-dependent endosomal sorting of clathrin-independent cargo by hook1. *J Cell Biol*. 2013;201:233–47.
52. Luiro K, Yliannala K, Ahtiainen L, Maunu H, Järvelä I, Kytälä A, Jalanko A. Interconnections of cln3, hook1 and rab proteins link batten disease to defects in the endocytic pathway. *Hum Mol Genet*. 2004;13:3017–27.
53. Villari G, Enrico BC, Del GM, Gioelli N, Sandri C, Camillo C, Fiorio PA, Bosia C, Serini G. Distinct retrograde microtubule motor sets drive early and late endosome transport. *Embo J*. 2020;39:e103661.
54. Sandvig K, Pust S, Skotland T, van Deurs B. Clathrin-independent endocytosis: mechanisms and function. *Curr Opin Cell Biol*. 2011;23:413–20.
55. Davidsson J, Puschmann A, Tedgård U, Bryder D, Nilsson L, Cammenga J. Samd9 and samd9l in inherited predisposition to ataxia, pancytopenia, and myeloid malignancies. *Leukemia*. 2018;32:1106–15.
56. Ma W, Huang G, Wang Z, Wang L, Gao Q. Irf7: role and regulation in immunity and autoimmunity. *Front Immunol*. 2023;14:1236923.

57. Zhao GN, Jiang DS, Li H. Interferon regulatory factors: at the cross-roads of immunity, metabolism, and disease. *Biochim Biophys Acta*. 2015;1852:365–78.
58. Salloum R, Franek BS, Kariuki SN, Rhee L, Mikolaitis RA, Jolly M, Utset TO, Niewold TB. Genetic variation at the irf7/phrf1 locus is associated with autoantibody profile and serum interferon-alpha activity in lupus patients. *Arthritis Rheum*. 2010;62:553–61.
59. Unterholzner L, Bowie AG. The interplay between viruses and innate immune signaling: recent insights and therapeutic opportunities. *Biochem Pharmacol*. 2008;75:589–602.
60. Salloum R, Niewold TB. Interferon regulatory factors in human lupus pathogenesis. *Transl Res*. 2011;157:326–31.
61. Wu M, Assassi S. The role of type 1 interferon in systemic sclerosis. *Front Immunol*. 2013;4:266.
62. Mishra S, Maurya VK, Kumar S, Ankita, Kaur A, Saxena SK. Clinical management and therapeutic strategies for the thyroid-associated ophthalmopathy: current and future perspectives. *Curr Eye Res*. 2020;45:1325–41.
63. Roy D, Ramasamy R, Schmidt AM. Journey to a receptor for advanced glycation end products connection in severe acute respiratory syndrome coronavirus 2 infection: with stops along the way in the lung, heart, blood vessels, and adipose tissue. *Arterioscler Thromb Vasc Biol*. 2021;41:614–27.
64. Géraud C, Koch PS, Goerdts S. Vascular niches: endothelial cells as tissue- and site-specific multifunctional team players in health and disease. *J Dtsch Dermatol Ges*. 2014;12:685–9.
65. Yang N, Sun H, Xue Y, Zhang W, Wang H, Tao H, Liang X, Li M, Xu Y, Chen L, Zhang L, Huang L, Geng D. Inhibition of magl activates the keap1/nrf2 pathway to attenuate glucocorticoid-induced osteonecrosis of the femoral head. *Clin Transl Med*. 2021;11:e447.
66. Baek SH, Kim KH, Lee WK, Hong W, Won H, Kim SY. Abnormal lipid profiles in nontraumatic osteonecrosis of the femoral head: a comparison with osteoarthritis using propensity score matching. *J Bone Joint Surg Am*. 2022;104:19–24.
67. Schepper JD, Collins F, Rios-Arce ND, Kang HJ, Schaefer L, Gardinier JD, Raghuvanshi R, Quinn RA, Britton R, Parameswaran N, McCabe LR. Involvement of the gut microbiota and barrier function in glucocorticoid-induced osteoporosis. *J Bone Min Res*. 2020;35:801–20.
68. Tian L, Wen Q, Dang X, You W, Fan L, Wang K. Immune response associated with toll-like receptor 4 signaling pathway leads to steroid-induced femoral head osteonecrosis. *Bmc Musculoskelet Disord*. 2014;15:18.
69. Ma M, Tan Z, Li W, Zhang H, Liu Y, Yue C. Osteoimmunology and osteonecrosis of the femoral head. *Bone Joint Res*. 2022;11:26–8.
70. Chen TT, Xiao F, Li N, Shan S, Qi M, Wang ZY, Zhang SN, Wei W, Sun WY. Inflammasome as an effective platform for fibrosis therapy. *J Inflamm Res*. 2021;14:1575–90.
71. Rabquer BJ, Tan GJ, Shaheen PJ, Haines GR, Urquhart AG, Koch AE. Synovial inflammation in patients with osteonecrosis of the femoral head. *Clin Transl Sci*. 2009;2:273–8.
72. Ren Y, Deng Z, Gokani V, Kutschke M, Mitchell TW, Aruwajoye O, Adapala NS, Kamiya N, Abu-Amer Y, Kim HK. Anti-interleukin-6 therapy decreases hip synovitis and bone resorption and increases bone formation following ischemic osteonecrosis of the femoral head. *J Bone Min Res*. 2021;36:357–68.
73. Gao Y, Xu X, Zhang X. Targeting different phenotypes of macrophages: a potential strategy for natural products to treat inflammatory bone and joint diseases. *Phytomedicine*. 2023;118:154952.
74. Luo Y, Yang Z, Zhao X, Li D, Li Q, Wei Y, Wan L, Tian M, Kang P. Immune regulation enhances osteogenesis and angiogenesis using an injectable thiolated hyaluronic acid hydrogel with lithium-doped nano-hydroxyapatite (li-nha) delivery for osteonecrosis. *Mater Today Bio*. 2024;25:100976.

Publisher's note

Springer Nature remains neutral with regard to jurisdictional claims in published maps and institutional affiliations.